small NANO MICRO

Layered Double Hydroxide-based Nanomaterials as Highly Efficient Catalysts and Adsorbents

Changming Li, Min Wei, David G. Evans, and Xue Duan*

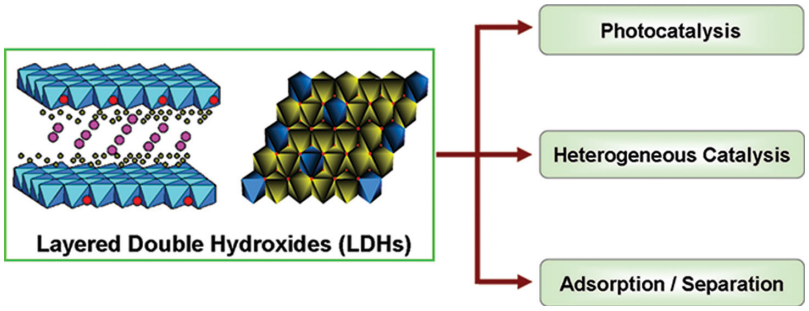

From the Contents

Layered double hydroxides (LDHs) are a class of anion clays consisting of brucite-like host layers and interlayer anions, which have attracted increasing interest in the fields of catalysis/adsorption. By virtue of the versatility in composition, morphology, and architecture of LDH materials, as well as their unique structural properties (intercalation, topological transformation, and self-assembly with other functional materials), LDHs display great potential in the design and fabrication of nanomaterials applied in photocatalysis, heterogeneous catalysis, and adsorption/separation processes. Taking advantage of the structural merits and various control synthesis strategies of LDHs, the active center structure (e.g., crystal facets, defects, geometric and electronic states, etc.) and macro–nano morphology can be facilely manipulated for specific catalytic/adsorbent processes with largely enhanced performances. In this review, the latest advancements in the design and preparation of LDH-based functional nanomaterials for sustainable development in catalysis and adsorption are summarized.

1. Introduction

Recent advances in synthetic nanoscience and nanotechnology have enabled progress in the development of novel catalysts and adsorbents applied in new energy conversion, green chemical industry, environmental cleaning, etc.[1] Indeed, the fascinating physical and chemical properties of the nano-sized materials arouse intense interest due to their superior catalytic and adsorbent behavior.[1e,2] Tremendous endeavor has been devoted to the control synthesis of various types of nano-sized catalysts/sorbents with desired structure and functionality.[1a,3] From the perspective of practical applications, a well-designed nano-catalyst/sorbent should involve the following issues: (i) How to achieve a high dispersion of active sites for the maximum utilization of material resources? (ii) How to tune the geometric and electronic state of active sites at the atomic scale for a high selectivity in specific industrial process? (iii) How to stabilize the obtained active sites for the long-term use and recyclability? Therefore, the development of material systems with tunable composition, size, structure and morphology, which satisfies these requirements simultaneously for specific catalysis/adsorption processes, remains a huge challenge.

Layered double hydroxides (LDHs), also known as hydrotalcite-like materials, are a class of 2D anionic clays consisting of positively-charged host layers and exchangeable interlayer anions, which can be expressed by the formula $[M^{2+}_{1-x}M^{3+}_{x}(OH)_2](A^{n-})_{x/n}\cdot mH_2O$ (M^{2+} and M^{3+} are divalent and trivalent metals, respectively; A^{n-} is the interlayer anion, as shown in **Figure 1**).[4] The unique supramolecular structure with the precisely-controlled chemical composition of both the inorganic layers and the interlayer gallery anions provides great potential to disperse and tune active sites at the atomic scale.[5] Moreover, the facile synthetic strategy (e.g., in-situ growth,[6] biological template,[7] electrochemical synthesis[8] can easily manipulate the LDH morphology on the micro-nano scale to stabilize the active motifs in the LDH layers or interlayer region during the catalytic/adsorbent process. In addition, the topotactic transformation property of the LDHs precursors to mixed metal oxides (MMOs) or metal/metal oxide composites upon calcination in an air/hydrogen atmosphere, respectively, can further improve the structure modulation strategies and thus expand the applied range of LDH materials as catalysts and adsorbents.[9] Therefore, the inherent merits of supramolecular structure, various synthesis approaches as well as the unique topotactic transformation behavior of LDH-based materials make them promising nanomaterial system for the fabrication of catalysts/adsorbents.

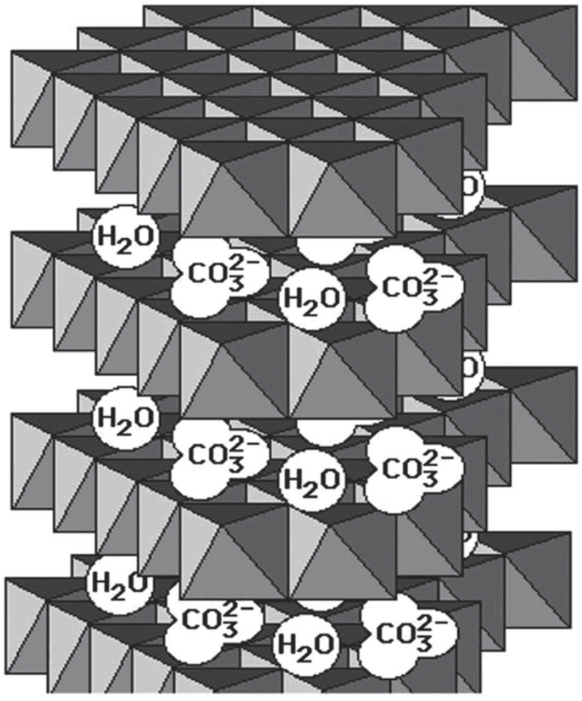

Figure 1. The structure of a layered double hydroxide, with interlayer carbonate anions. Reproduced with permission.[4d] Copyright 1999, Elsevier.

In this review, we comprehensively summarize recent progress in the design and preparation of LDH-based nanomaterials, which have been applied in the fields of catalysis and adsorption. The structure design, controlled synthesis of LDHs and their derived nanocomposites as well as their catalytic (including photocatalysis and heterogeneous catalysis) and adsorbent functionality are reviewed in detail. Moreover, the relationship between the modulation of active center structure (e.g., crystal facets, defects, geometric and electronic states) and the enhanced catalytic/adsorbent performance is emphasized. In the final section, current challenges and future strategies are discussed from the viewpoint of material design, structure–property correlation and practical applications for catalytic/adsorbent processes. It is anticipated that this review will attract more attention toward LDH functional nanomaterials for sustainable development in the field of catalysis/adsorption and encourage future work to push forward the advancement of this fast-growing area.

2. LDH-Based Nanomaterials in Photocatalysis/Photoelectrocatalysis

The conversion of solar energy into clean chemical reagents and fuels by the photocatalytic process to solve the global energy problem is one of the most important fields in the 21st century.[10] From the viewpoint of semiconductor photochemistry, photoexcitation of electrons (e^-) and holes (h^+) occurs when the energy of the incident photons matches or exceeds the band gap of the semiconductor. Some electrons/holes will interact with electron acceptors/donors adsorbed on the surface of photocatalysts to participate in the photochemical reaction process. However, most of them undergo

Dr. C. M. Li, Prof. M. Wei, Prof. D. G. Evans, Prof. X. Duan
State Key Laboratory of Chemical Resource Engineering
Beijing University of Chemical Technology
Beijing 100029, PR China
E-mail: weimin@mail.buct.edu.cn

DOI: 10.1002/smll.201401464

NANO MICRO small

recombination non-radiatively or radiatively, resulting in heat or photoemission, respectively, which decreases the photocatalytic efficiency.[10c] Therefore, the major challenge of the phototransformation process is to design and prepare novel nanomaterials that possess a high charge-hole separation and thus good photocatalytic performance under the light (especially visible light) radiation. The choice of photoactive motifs (e.g., Ti, Cr, Zn) incorporated into LDH matrix as well as the facile structure modulation in micron/nano/atom scale provide the great potential to fabricate LDH-based photocatalysts with desired behavior.

2.1. LDHs Themselves as Photocatalysts

The metal doping in the primary semiconductor materials is one of the effective strategies to improve the efficiency of charge-hole separation in the field of photocatalysis research. For LDH materials, their unique photocatalytic properties have been mostly ignored for a long time. Until 2009, García et al.[11] developed the concept that LDH materials serve as doped semiconductors, in which the metal element type and proportion can be facilely controlled. For instance, when the higher valent metal is titanium or when the divalent metal is zinc, LDH materials analogous to titania or zinc oxide can be obtained with the advantage that the "dopant" metal would be present in a well-defined structural position. In this way, the location of dopant on semiconductor oxides can be precisely determined in LDHs. Their studies also confirmed that Zn- and Cr-containing LDHs are highly active for the photocatalytic O_2 generation from water in the visible region with an apparent quantum yield as high as 60.9% at 410 nm, which show the vast potential of LDHs as visible light photocatalysts. This work evokes great research interest in LDH materials as photocatalysts, and various new photocatalytic materials such as binary (e.g., CoFe-LDHs[12] or ternary LDHs (e.g., NiZnCr-LDHs,[13] FeMgAl-LDHs[14] were developed in recent years.

Our group[15] gives a further insight into the photocatalytic properties of LDH materials. The photoactive site (e.g., CrO_6 or TiO_6 octahedron unit), can be highly dispersed in the LDH matrix (**Figure 2**). The resulting structure would enhance the efficiency of charge-hole separation and improve photoconversion capability with visible-light irradiation. To confirm this point, a series of Cr- or Ti-containing LDH materials were synthesized by a simple and scale-up co-precipitation method, which display remarkable photocatalytic performance in visible light. Especially, the Ti-containing LDH displays a largely enhanced photocatalytic activity with an H_2-production rate of 31.4 μmol h^{-1} as well as good recyclable performance for water splitting, which is 18 times higher than that of $K_2Ti_4O_9$. The structural characterization and DFT calculations verified the high dispersion of TiO_6 octahedra in the LDH matrix by the formation of an M^{2+}–O–Ti network with the significant depression of electron–hole recombination, accounting for its good water splitting behavior. The self-doping of defect sites (e.g., Ti^{3+}) in LDHs themselves may also have great impact on the efficiency of charge-hole separation for photocatalysis. Recently, we[16] reported the tuning of Ti^{3+} defect type and concentration in Ti-based LDH materials by the manipulation of their size, shape and morphology via a bottom-up synthesis approach, which enhanced both the efficiency of electron–hole separation and the resulting photocatalytic performance. It was demonstrated that the density of Ti^{3+} defects increases gradually along with the decrease of NiTi-LDH nanosheets from 90 to 30 nm, which results in an effective electron–hole separation as confirmed by the photoluminescence, ESR and EXAFS measurements. It is worth noting that the M^{2+}/M^{3+} ratio of LDH materials imposes a great influence on their photocatalytic performances. An appropriate aggregation of active component (normally semiconductor components) in the support matrix would modify the electronic structure and band gap of LDH materials, which is favorable for a highly-efficient electron-hole separation and the resulting catalytic behavior.

Besides the defect sites, the specific metal ion or base site in the LDH layers can also act as co-catalysts

Min Wei obtained her BEng degree in 1995 and MEng degree in 1998 from Beijing University of Chemical Technology (BUCT). She subsequently received her PhD from Peking University in 2001, after which she joined the staff of BUCT. She was promoted to full Professor in 2005. She was a visiting scholar in the Georgia Institute of Technology in 2008. Her research interests focus on inorganic–organic composite functional materials as well as new catalysts.

David G. Evans studied as both an undergraduate and a research student at Jesus College, Oxford, and obtained a DPhil under the supervision of Prof. D. M. P. Mingos FRS. After postdoctoral work at Bristol University with Prof. F. G. A. Stone FRS, he was appointed as a lecturer at Exeter University in 1985. Several visits to Chinese university chemistry departments in the early 1990s convinced him of China's great potential for development and he moved to Beijing University of Chemical Technology in 1996. His research interests focus on intercalation in layered solids.

Xue Duan was elected as an Academician of the Chinese Academy of Sciences in 2007. He was awarded his BS degree from Jilin University and MS and PhD degrees from Beijing University of Chemical Technology (BUCT). He was subsequently appointed to the staff of BUCT and established the Applied Chemistry Research Institute in 1990. He was promoted to full Professor in 1993 and to PhD supervisor status in 1995. He is currently Director of the Institute of Applied Chemistry and Executive Vice-Chair of the Academic Committee of the State Key Laboratory of Chemical Resource Engineering.

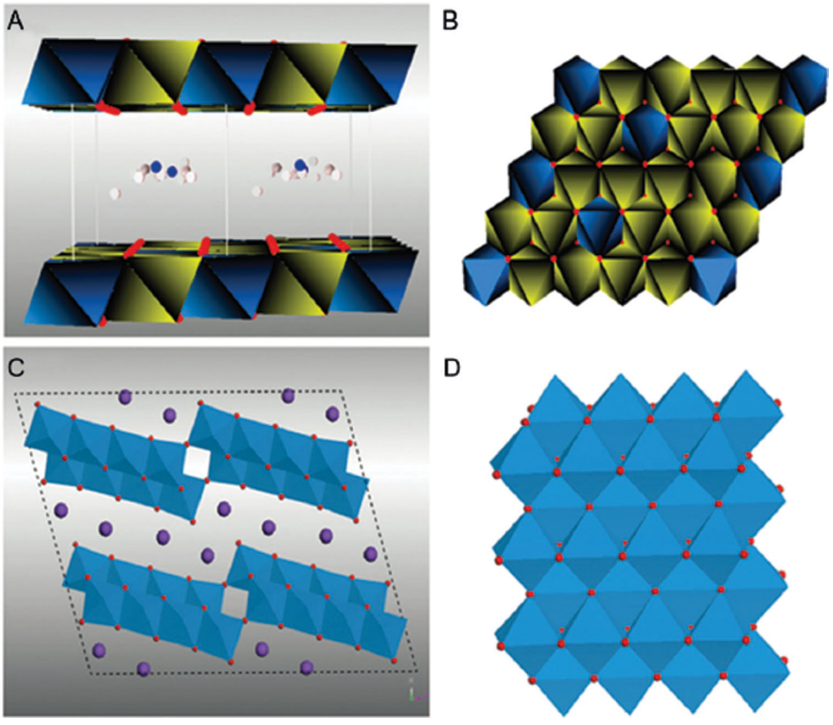

Figure 2. (A) A polyhedral representation of the LDH structure showing the metal hydroxide octahedra stacking along the crystallographic *c* axis. Water and anions are present in the interlayer region. (B) Vertical view of the surface atomic configurations for the LDH layer. Dark blue: Ti; yellow: Ni. (C) Crystal structure of $K_2Ti_4O_9$. D) Vertical view of the surface atomic configurations for the TiO_6 octahedra in $K_2Ti_4O_9$. Reproduced with permission.[15a] Copyright 2012, Wiley.

in some photosynthesis process such as the photocatalytic conversion of CO_2. Izumi et al.[17] developed the copper-modified LDHs located both at the host layers (denoted as $[Zn_{1.5}Cu_{1.5}Ga(OH)_8]^+_2(CO_3)^{2-}\cdot mH_2O$) and in the interlayer gallery (denoted as $[Zn_3Ga(OH)_8]^+_2[Cu(OH)_4]^{2-}\cdot mH_2O$), which showed activity for the photoconversion of CO_2 in the presence of H_2. The Cu species was supposed as the active site along with LDH as the solid-base adsorbent for CO_2, whose proposed reaction mechanism is shown in **Figure 3**. Inspired by the aldol reaction of carbonyl compounds over MgAl-LDHs in aqueous solution, Tanaka et al.[18] further suggested that the surface base sites of LDHs with a high water tolerance act not only as CO_2 adsorbent but also as active sites for the activation of CO_2 under photoirradiation. They confirmed that the photocatalytic conversion of CO_2 occurs over various LDHs such as NiAl-LDHs, ZnAl-LDHs, NiGa-LDHs, ZnIn-LDHs and even MgAl-LDHs, which significantly expands the photocatalytic application of LDH materials.

2.2. LDH-Based Nanocomposites as Photocatalysts

Another strategy to improve the utilization efficiency of photo-excited electrons and holes in photochemistry is the recombination of primary LDHs with other functional units to form composite nanomaterials. Assembly of LDHs with other inorganic semiconductors is an effective method to take full use of their synergy effect.[19] As a typical example, Hwang et al.[20] recently reported the synthesis of mesoporous

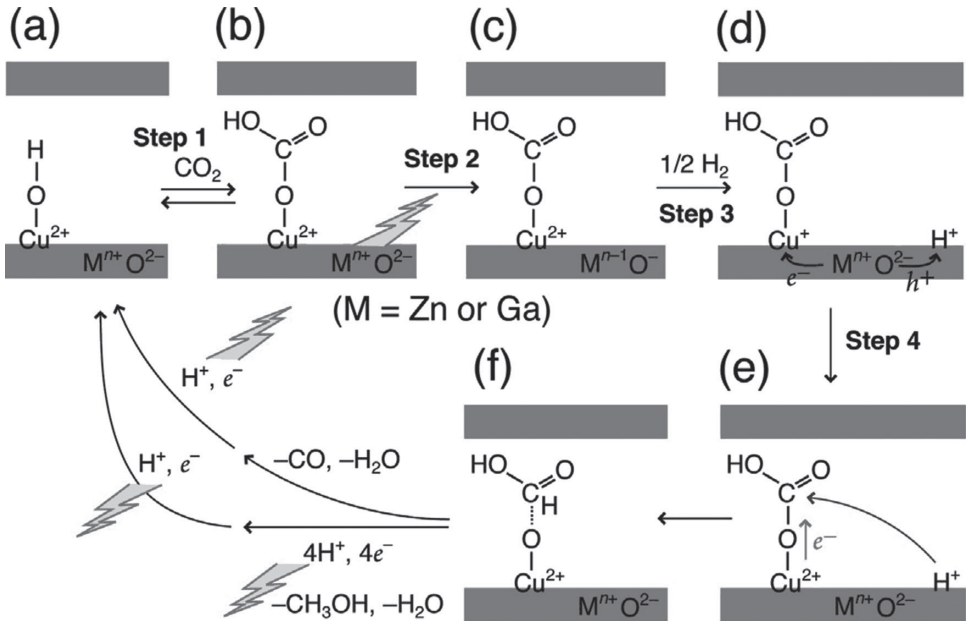

Figure 3. Proposed photocatalytic cycle of CO_2 reduction to methanol or CO using LDH catalysts consisting of Zn, Ga and interlayer Cu sites. Reproduced with permission.[17b] Copyright 2014, Elsevier.

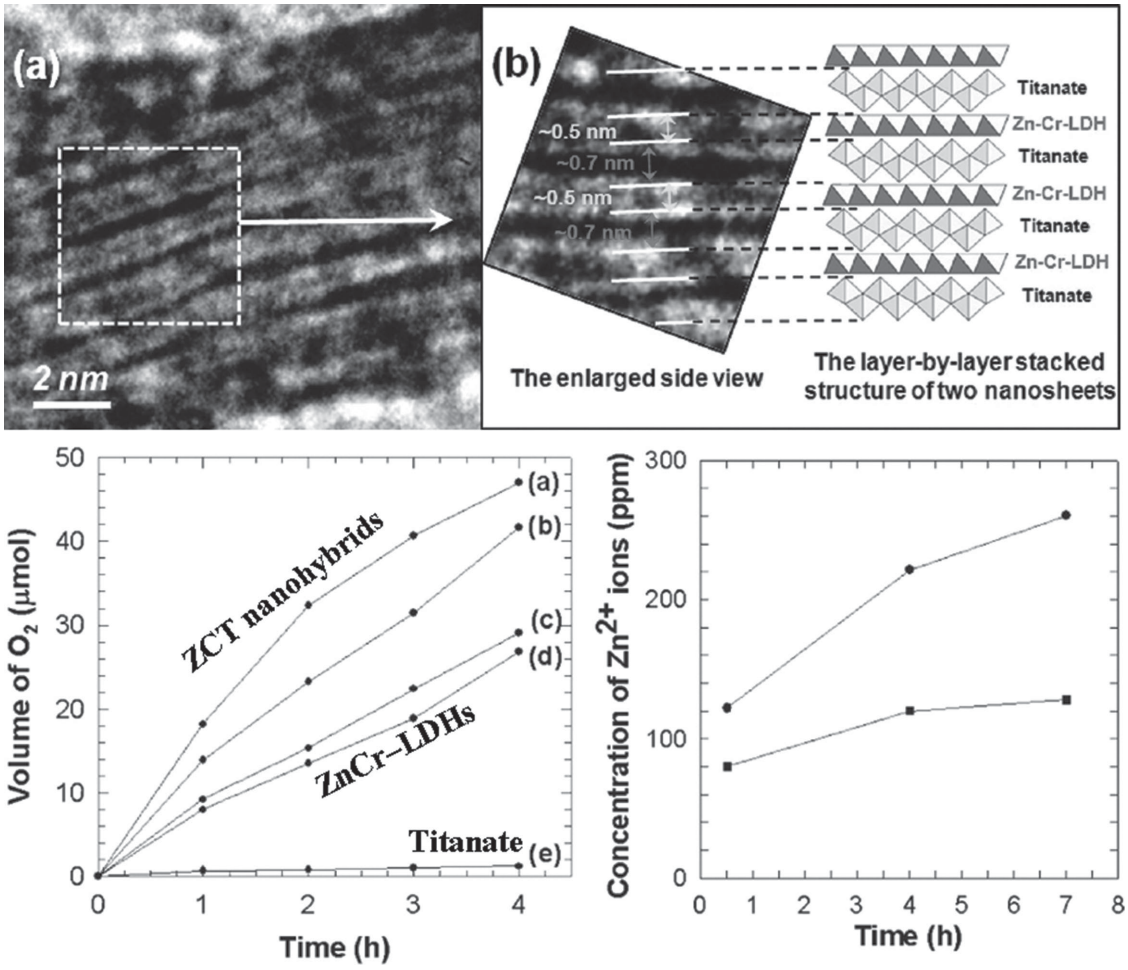

Figure 4. The as-synthesized mesoporous layer-by-layer ordered nanohybrids by self-assembly between oppositely-charged 2D nanosheets of ZnCr-LDH and their high activity for visible light-induced O_2 generation from water. Reproduced with permission.[20] Copyright 2011, American Chemical Society.

layer-by-layer ordered nanohybrids by self-assembly between oppositely-charged 2D nanosheets of ZnCr-LDH and layered titanium oxide for visible light-induced O_2 generation from water (**Figure 4**). The obtained heterolayered nanohybrids show a strong absorption of visible light and a remarkably depressed photoluminescence signal, indicating an effective electronic coupling between the two component nanosheets. The resultant nanohybrids are fairly active for visible light-induced O_2 generation with a rate of ~1.18 mmol h^{-1} g^{-1}. Furthermore, the chemical stability is significantly improved as the result of the protection of LDH lattice by highly-stable titanate layer, which is superior to the pristine ZnCr-LDH material under the same experimental conditions.

Recently, some attempts have been made to combine LDHs with graphene to enhance the photocatalytic performances owing to the excellent carrier transportation capability of graphene and its ability to induce visible-light responsive activity. The nanohybrids of LDHs and graphene are supposed to create a strong physical contact, which can act as a good acceptor for photoinduced electrons and thus reduce the e–h recombination. Our group[21] reported the fabrication of NiTi-LDH/reduced graphene oxide (RGO) composite materials via an in situ growth method; the resulting NiTi-LDH/RGO composite displays enhanced photocatalytic activity toward water splitting into oxygen with a rate of 1.968 mmol g^{-1} h^{-1} and a quantum efficiency as high as 61.2% at 500 nm, which is among the most effective visible light photocatalysts (**Figure 5**). Electron spin resonance (ESR) and Raman scattering spectroscopy confirm the electrons transfer from NiTi-LDH nanosheets to RGO with an efficient separation of electron–hole pairs indicated by the photoluminescence (PL) measurements, accounting for the strong carrier mobility and the resulting largely-enhanced photocatalytic activity in comparison with pristine NiTi-LDH material. Moreover, further work on the tuning of type/morphology of both LDHs and graphene gives rise to improved photocatalytic performance of these nanocomposites (e.g., ZnCr-LDHs/RGO[22] and ZnAl-LDHs/carboxyl graphene.[23]

The topotactic transformation of LDH precursor materials to mixed metal oxides (MMOs) is an alternative way to establish efficient nanocomposites for photocatalysis. The MMO materials can inherit the LDH precursor morphology with photoactive nanoparticles (e.g., ZnO, TiO_2) highly-dispersed in the calcined matrix, which provide

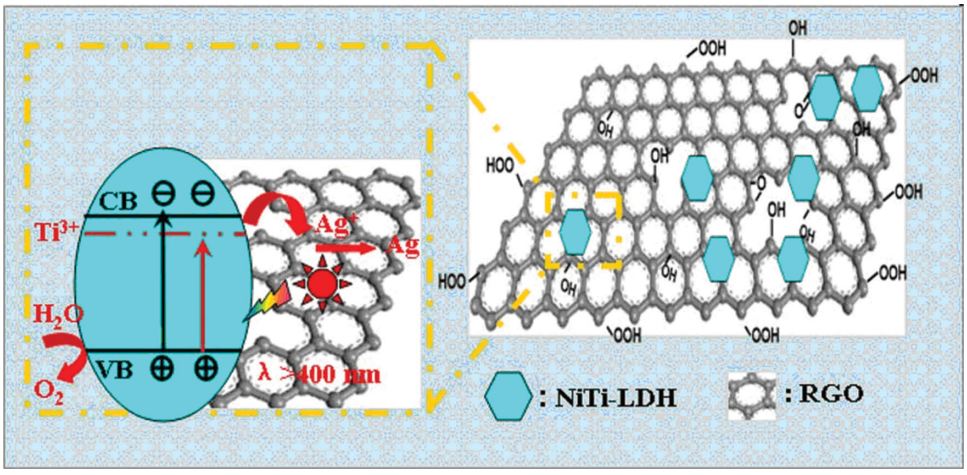

Figure 5. The fabrication of NiTi-LDG/RGO composite materials via an in situ growth method as the visible-light-responsive photocatalysts toward water oxidation. Reproduced with permission.[21] Copyright 2013, American Chemical Society.

sufficient active surface area and high adsorption capacity for photodegradation processes. We[7] reported a biomorphic hierarchical MMO framework through a biotemplated synthesis method. A uniform Al_2O_3 coating was deposited on the surface of the biotemplate with an atomic layer deposition (ALD) process; the film of ZnAl-LDH, which faithfully inherits the surface structure of the biotemplate, was prepared by an in situ growth technique. Subsequently, a polycrystal ZnAl-MMO framework obtained by calcination of the ZnAl-LDH precursor was demonstrated as an effective and recyclable photocatalyst for the decomposition of dyes in water, owing to its rather high specific surface area and hierarchical distribution of pore size. Most notably, shape-controlled synthesis of nanocrystallines with exposed active facets can also be achieved via the topotactic transformation process of LDHs. Our group[24] further reported ZnO nanoplatelets with a high exposure of (0001) facet embedded on a hierarchical flowerlike matrix, which were achieved via the in situ topotactic transformation of a ZnAl-LDH precursor. The hexagonal crystals of ZnAl-LDH nanoflakes serve as both a ZnO source and a rigid template, which restrains the fast growth rate of ZnO along the *c*-axis and induces the preferred growth of the nanoplatelets along the $[10\bar{1}0]$ direction. The resulting ZnO/Al_2O_3 nanocatalyst displays well visible-light photocatalytic activity towards the degradation of Rhodamine-B with good stability and recyclability in aqueous solution, which can be attributed to the enhanced separation efficiency of electron–hole pairs resulting from the oxygen defect-riched ZnO nanoplatelets. In addition, other nanocomposites such as the recombination of the metal nanoparticles, quantum dot with LDH or MMO materials have also been developed for good photocatalytic performances.[25]

2.3. LDH Materials in Photoelectrocatalysis

The coupling photochemistry with electrochemistry (denoted as photoelectrochemistry) is the latest developed technology to improve the efficiency of both the photocatalysis and electrocatalysis process applied in the new energy field.[26] The typical example is the photoelectrochemical (PEC) splitting of water into hydrogen and oxygen by the direct use of sunlight, which has aroused extensive interest in recent years. The integration of promising water oxidation electrocatalyst with a photon-absorbing substrate can provide a substantial reduction in the external power needed to drive water splitting. By virtue of the versatility in structural morphology of nanostructured LDHs (e.g., high surface-to-volume ratio, short diffusion length for carrier transport), we reported[27] the design and fabrication of a sophisticated nanoarray structure consisting of the semiconductor ZnO core–hierarchical LDH shell as photoelectrodes for the PEC catalysis (**Figure 6**). The core-shell structure shows the following advantages: (i) the semiconductor core guarantees the utilization of solar energy, giving rise to reduced external power consumption; (ii) the LDH shell as effective co-catalyst increases the reaction kinetics, thus depressing the charge recombination rate; (iii) the hierarchical structure enables a convenient charge transfer to the electrode/electrolyte interface where the oxidation of water molecules occurs. The resulting ZnO@CoNi–LDH nanoarray material exhibits promising behavior in PEC water splitting, giving rise to a largely-enhanced photocurrent density as well as stability, much better than those of ZnO-based photoelectrodes. This is attributed to the successful integration of photogenerated electron–hole separation originating from the ZnO core and the good electrocatalytic activity of LDH shell.

Similar to the single photocatalytic process, the topotactic transformation of LDH precursor materials is another choice to modify the active sites by doping for improved PEC effect. Lee et al.[28] reported that MMO nanostructures co-doping with carbon and nitrogen were synthesized by annealing a terephthalate intercalated LDH precursor under ammonia gas flow. The LDH interlayer gallery allows effective access of NH_3 and carbon source to its crystal lattice for a uniform nitrogen and carbon doping. Such co-doped MMO material exhibits significantly red-shifted absorption to visible light region relative to pure MMO. PEC water oxidation and

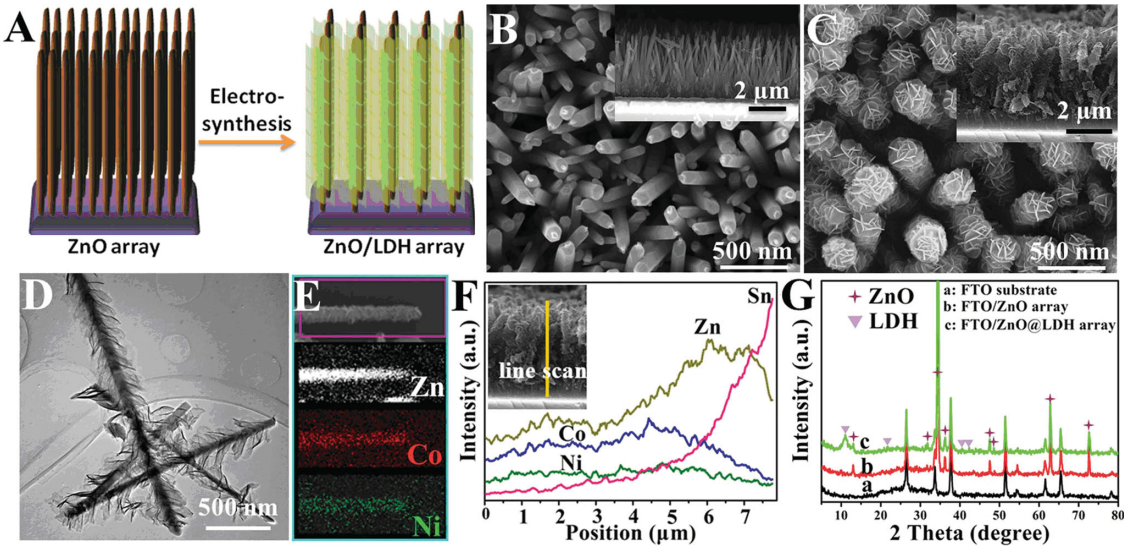

Figure 6. (A) Schematic illustration of the fabrication of ZnO@LDH core–shell NWs array; SEM images of (B) ZnO NWs and (C) ZnO@LDH core–shell NWs array on FTO; (D) TEM image, (E) EDX mapping and (F) line scan results of ZnO@LDH core–shell NWs array; (G) XRD patterns of (a) FTO substrate, (b) ZnO NWs array on FTO, (c) ZnO@CoNi-LDH NWs array on FTO. Reproduced with permission.[27] Copyright 2014, Wiley.

incident-photon-to-current-conversion efficiency of LDH-derived photocatalysts demonstrate that the visible light absorption caused by the nitrogen atom doping contributes to the photocatalytic activity over the absorbed wavelength range (<610 nm). Density functional theory calculations of electronic structures further elucidate the possibility of bandgap narrowing upon nitrogen and carbon co-doping into MMO structures. Owing to the bifunctional properties of both photocatalytic and electrocatalytic activity for LDH-based materials, it thereby gives great opportunities for scientists to design and fabricate novel photoelectrocatalysts. As a booming filed, we believe that more exciting results will emerge for photoelectrocatalysis over well-designed LDH-based materials in the near future.

3. LDH-Based Heterogeneous Catalysts

Traditionally, LDHs have been widely used as heterogeneous catalysts for base-catalyzed reactions or redox transformations.[29] Recently, by virtue of the versatility of LDH materials (e.g., intercalation, delamination, lattice orientation, topotactic transformation), various catalytically-active transition metal species (e.g., Fe, Co, Ni, V, Cu, Rh) can be incorporated into LDH precursors. These features make LDH-based materials display great potential in heterogeneous catalysts with high dispersion, preferential orientation as well as good catalytic behavior (activity, selectivity and stability of active sites).

3.1. The Catalytically-Active Species Immobilized in LDH Interlayer Gallery

Although homogeneous catalysts show great merits in the accessibility of catalytic sites, tunability in chemo-, regio- and enantioselectivity, the resulting high catalytic activity and selectivity, the employment of expensive and toxic organic metallic reagents as well as the difficulty in catalytic separation/recylability restrict their commercial applications.[30] Taking advantage of the intercalation property of LDH materials, a variety of active species in homogeneous catalysis (e.g., inorganic anions, organic acid/base and organic complexes) can be intercalated into the LDH gallery, which gives the chance to heterogenize the homogeneous reaction process over LDH-based catalysts with enhanced lifetime, thermal stability and facile separation/purification. Moreover, LDHs themselves offer a number of advantages as hosts: the electrostatic interactions between LDH layers and catalytically-active anions can induce an ordered arrangement of interlayer species and tailor the orientation of active sites; the distribution of active sites can be controlled by modulating the charge density of host layers (which depends on the ratio of M^{II} to M^{III} cation); the host-guest interaction between LDH layers and catalytically-active anions would also lead to an increase in the catalyst stability.

The inorganic active species immobilized in LDHs is the earliest developed heterogeneous catalysts. Sels et al.[31] firstly reported the synthesis of tungstate intercalated LDH (WO_4^{2-}-LDHs) as a biomimetic catalyst for mild oxidative bromination. Subsequently, more advanced polyoxometallate (POM) and other inorganic active species intercalated LDHs have also been developed as oxidation catalysts towards various kinds of oxidizing reactions, i.e., LDH-WO_4^{2-} for N-oxidation of aliphatic tertiary amines,[32] $K_{11}WM_3(H_2O)_2O[ZnW_9O_{34}]_2{\cdot}44H_2O$ (K–$Zn_2M^{III}{}_3WO$; M^{III} = Fe^{3+}, Mn^{3+}) intercalated LDHs for the oxidation of aromatic aldehydes,[33] the generation of singlet molecular oxygen from H_2O_2 over MoO_4^{2-} intercalated MgAl-LDHs.[34] Moreover, the host LDH layers not only act as anchor sites for active anions, but also play the role of co-catalyst for organic reactions. Li et al.[35] reported that a series of polyoxometalate (POM) intercalated LDH catalysts exhibit base-synergistic catalysis towards epoxidation of allylic alcohols without using organic solvent (**Figure 7**). The cooperation between

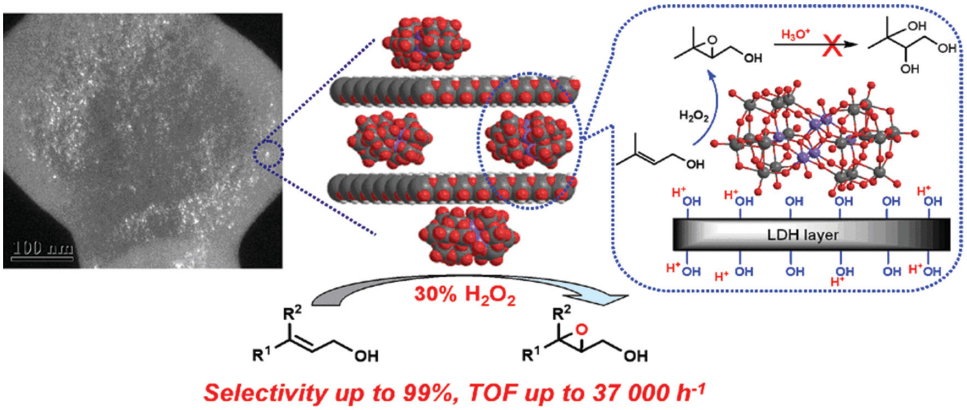

Figure 7. The as-synthesized polyoxometalate (POM) intercalated LDH nanomaterials as base-synergistic catalysts toward the epoxidation of allylic alcohols. Reproduced with permission.[35] Copyright 2009, Elsevier.

the POM guest and LDH host achieves satisfactory catalytic behavior (selectivity of epoxide: 99%; H_2O_2 efficiency: 95%; TOF: 37 200 h^{-1}) without the need of base additives and pH controlling; the LDH–POM catalysts can be readily recycled with no apparent loss of catalytic performance. The extremely higher epoxide selectivity of the heterogeneous LDH–POM catalysts than the corresponding homogeneous Na–POM ones is attributed to the beneficial effect of basic LDH host on the suppression of the acid-catalyzed epoxide hydrolysis.

The organometallic complexes can also be intercalated in the LDH gallery as heterogeneous catalysts, which demonstrate the great potential for LDHs as the carrier to immobilize the active species used in homogeneous catalysis. Various intercalated metal complexes in LDHs have been reported to afford enhanced catalytic activity in a number of catalytic processes, including the hydroformylation of higher olefins over rhodium complex intercalated in ZnAl-LDHs,[36] epoxidation by salen–Mn(III) (salen = *N,N′*-ethylenebis(salicylimine)),[37] Ti(IV)-Schiff base complex,[38] or iron(III) porphyrins intercalated LDHs.[39] Cu(II) complexes[40] and La(III) hydroxy citrate complexes[41] intercalated LDHs have been reported to catalyze the peroxidative oxidation of alkanes and the transesterification reaction of 1-phenylethanol with enhanced catalytic activity and good recyclability. Furthermore, an increase in enantioselectivity was observed over chiral metal complex intercalated LDH materials, as reported by Anderson's group[42] and He's group,[43] owing to the controlled orientation and/or dispersion degree of the intercalated active species. As an example, He et al.[43a] recently reported that vanadium(V) and zinc(II) coordinate to the pre-intercalated α-amino anions in LDH gallery, showing significantly-enhanced enantioselectivity in the asymmetric epoxidation. The catalytic behavior and DFT calculations indicate that the steric hindrance of LDH layer improves the enantioselectivity by facilitating the formation and stability of the preferable catalytic transition state.

Although great progresses have been made for the intercalation of homogeneous active anions in LDHs as heterogeneous catalysts, it is most likely that the adsorbed active species on the particle surface gives a predominant contribution to the catalytic reaction. A large diffusion resistant of reactants into the LDH gallery would to some extent decrease the utilization of interlayer active anions. Moreover, many active species can not be intercalated into LDH gallery owing to their large size and/or low charge density. To solve these problems, the delamination of LDH microcrystals to ultra-thin nanosheets as carriers for the immobilization of active species would be an effective strategy. Recently, He et al.[43c] compared the catalytic performance of three catalysts towards asymmetric epoxidation of allylic alcohols with tert-butyl hydroperoxide (ButOOH): a homogeneous vanadium(V) complex, the one intercalated in a ZnAl-LDH host, and immobilized on LDH nanosheets (**Figure 8**). It was found that the intercalation of amino acid ligands (intercalated LDH sample) leads to

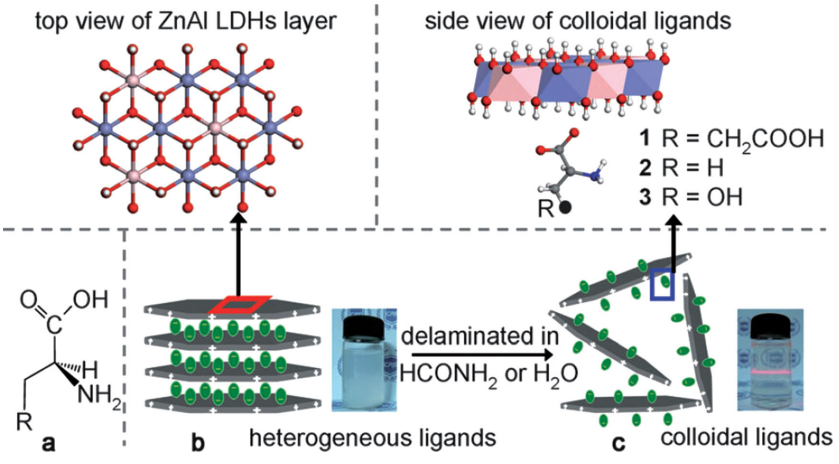

Figure 8. Intercalation of α-amino acids (1: *L*-glutamic acid; 2: *L*-alanine; 3: *L*-serine) (a) in an LDH host gives a heterogeneous catalyst precursor (b), whilst immobilization on delaminated LDH nanosheets gives a pseudo-homogeneous catalyst precursor (c). The materials obtained by treating (a)–(c) with VO(OPri3) were used as catalysts for the asymmetric epoxidation of allylic alcohols with ButOOH. Reproduced with permission.[43c] Copyright 2011, Wiley.

NANO MICRO small

a significant increase in the enantiomeric selectivity but a low reaction rate compared with the homogeneous catalyst. This can be attributed to the access of reactant molecules to the active sites being restricted and/or directed by the rigid inorganic layers. Immobilization of the vanadium (V) complex onto LDH nanosheets (delaminated LDH sample) allows the catalytic reaction occur under pseudo-homogeneous conditions, thereby remarkably increasing the reaction rate while maintaining a high enantioselectivity. Most notably, the pseudo-homogeneous catalyst was also used in water medium with good activity, and the colloidal catalyst was separated from the products by simple liquid/liquid separation more easily than in organic solvents. The catalysts can be recycled and reused with no obvious loss of catalytic activity and enantioselectivity. As demonstrated in this example, the immobilization of homogeneous species on the delaminated LDH nanosheets would break through the restrictions of active species size and diffusion kinetic, which shows great potential to construct LDH-based heterogeneous catalysts.

3.2. LDHs as Supports for Metal Nanocatalysts

As an outstanding substitution of homogeneous metal complexes, metal nanocatalysts have attract a intense research interests owing to their distinguishing structural advantage (e.g., high active surface area, surface effect, and size effect) as well as promising catalytic performances.[44] For LDH materials, they can serve as supports for metal nanocrystallines, which prevent the sintering/aggregation of metal nanoparticles by means of an exterior confinement effect from the LDH layers. Moreover, as the traditional solid base catalysts, LDH host layers can provide base sites that impose a synergistic effect with the supported metal particles for enhanced catalytic behavior.

The metal nanoparticles supported on LDH materials generally exhibit strong support- determined feature of the morphology and size, which is the key factor contributing to enhanced activity and selectivity of catalysts.[45] Li et al.[46] developed a new precipitation–reduction method to synthesize LDH-supported Pd catalysts with either tetrahedral or octahedral morphology. It was found that the tetrahedral particles with only exposed Pd(111) facet showed higher selectivity towards ethylene than truncated octahedral Pd particles enclosed by both Pd(111) and Pd(100) facets in the selective hydrogenation of acetylene. Zhang et al.[47] further demonstrated the preferential deposition of gold nanoparticles (Au NPs) with a narrow size distribution (2–3 nm) on the lateral $(10\bar{1}0)$ facets of LDH platelets. The crystal face features of LDH platelets impose a crucial effect on the location and particle size of Au NPs. The lateral $(10\bar{1}0)$ facet with a high density of dangling bonds may have relatively active chemical characteristics, resulting in the preferential deposition of Au NPs on the $(10\bar{1}0)$ facet. Most recently, Jung et al.[48] reported the synthesis of Pt nanoparticles immobilized on exfoliated MgAl-LDH nanosheets via an electrostatic self-assembly between negatively-charged Pt NPs and positively-charged LDH nanosheets (**Figure 9**). The LDH nanosheets provide double sides of hydroxide functionality to stabilize Pt NPs, and facilitate a fast diffusion of reactants into the catalyst surface. The Pt-LDH nanosheets catalyst exhibits an improved reaction rate, turnover frequency and reaction durability toward the reduction of *p*-nitrophenol into *p*-aminophenol by $NaBH_4$, maintaining more than 97% of catalytic conversion.

In some cases, the transition metal cations in LDH host layers (e.g., Ru^{3+}, Rh^{3+}, Co^{2+}, Cu^{2+}) also act as active species for catalytic oxidation reactions.[49] A high dispersion of these cations in the non-active LDH matrix would significantly enhance the catalytic property. As a typical example, Asefa et al.[50] reported the catalytic performances of ZnCo-LDHs toward water electrooxidation. The high dispersion of Co^{3+} combined with the synergistic effect of Zn component in LDH layers accounts for the more than 10 times higher TOF per Co atom than the counterparts (e.g., $Co(OH)_2$ and Co_3O_4). Owing to these active sites on the LDH layers, the host layers themselves not only act as a support for metal nanocatalysts, but also play the role of cocatalyst for catalytic reactions. Hensen et al.[51] reported the synthesis of Au/

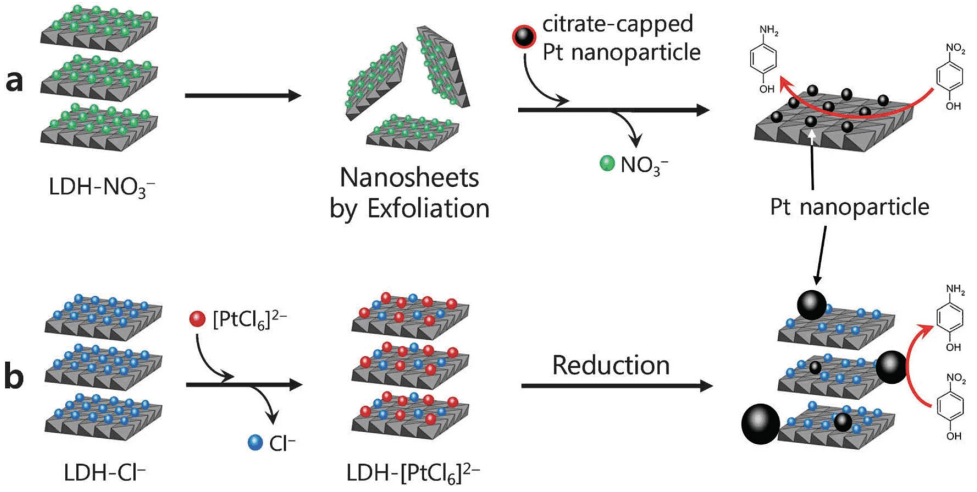

Figure 9. Schematic representations for the syntheses and the catalytic reactions of (a) ex-LDH–Pt and (b) in-LDH–Pt. Reproduced with permission.[48] Copyright 2014, Wiley.

chromium (III)-containing hydrotalcites as the synergetic catalyst toward liquid-phase aerobic oxidation of alcohols in the absence of base additives. It was found that Au/MgCr-LDH gave a significantly higher benzaldehyde yield (76%) and TOF (1880 h^{-1}) than other transition metal-containing LDH-based catalysts. The high activity of MgCr-LDH as a support was attributed to the fact that both the surface basic sites and chromium participate in alcohol dehydrogenation. Most recently, Zhang et al.[52] prepared ultrafine Au nanoclusters (~1.5 nm) supported on M_3Al-LDHs (M = Mg, Ni, Co) by using water-soluble glutathione-capped Au nanoclusters as precursor. Owing to the basic sites provided by the LDH layers, these catalysts present considerably high activities for a wide range of alcohols oxidation reactions without basic additives. The presence of transition metal cations (Ni^{2+}, Co^{2+}) in the LDH supports was confirmed to enhance the catalytic activity over Au NPs/Ni_3Al-LDH and Au NPs/Co_3Al-LDH samples. Specially, the Au NCs/Ni_3Al-LDHs exhibits the highest activity for the aerobic oxidation of 1-phenylethanol (TOF: 46 500 h^{-1}) under solvent-free conditions, which is attributed to the strongest Au–support synergistic effect among the studied catalysts.

3.3. Metal Nanocatalysts Based on Topological Transformation of LDHs

The topological transformation of the LDH precursors containing VIII element (e.g., Fe, Co, Ni) or some noble metals (e.g., Pd) offers a facile strategy to prepare supported metal nanocatalysts.[53] The resulting catalysts can inherit the morphology of LDH precursors with metal nanoparticles embedded in the calcined LDH matrix after the topological transformation process in hydrogen atmosphere, which would guarantee a high dispersion of metal nanoparticles and anti-sintering ability. Moreover, the architectural feature of polynary LDH precursors with the uniformly-distributed M^{II} and M^{III} cations in hydroxide layers should facilitate the design and preparation of supported bimetal nanocatalysts with tunable geometric and electronic structure.

Wei et al.[9,54] firstly reported that well-dispersed and embedded Fe, Co, Ni metal nanoparticles were obtained by the reduction of LDH precursors, especially for the metallic iron nanoparticles with a high density (10^{14} to 10^{16} m^{-2}) and good thermal stability (up to 900 ºC) by using MoO_4^{2-}-intercalated FeMgAl-LDHs as a precursor. These catalysts are highly active for the formation of single-walled carbon nanotube (SWNT)-array double helices, and exhibit notable anti-sintering of metal nanoparticles for the pyroreaction. Zhang et al.[55] further reported the preparation of a high loading and well-dispersed Ni catalyst by using NiAl-LDHs as a precursor, which showed well catalytic behavior toward the decomposition of hydrazine hydrate ($N_2H_4{\cdot}H_2O$) at room temperature (100% conversion and 93% H_2 selectivity) with the synergistic effect of basic sites from the calcined support.

The calcination temperature and heating rate have significant influences on the structure of calcination products.[56] A high temperature (normally above 450 ºC) will definitely cause the phase segregation and the formation of spinel, particularly for transition metal-containing LDHs. A fast heating rate would lead to the disruption of topotactic transformation process owing to the quick shrinking of the volume. For example, the NiAl-LDHs sample can be easily reduced at below 400 ºC; while a calcination at 450 °C induces the generation of NiO and partial spinel phase, which increases the reduction temperature to as high as 630 °C.[6,57] Therefore, a careful control over calcination temperature and heating rate is necessary to obtain the desired structure. Recently, our group[58] developed a surface defect-promoted Ni nanocatalyst via an in situ slow reduction process (2 ºC/min) with a high dispersion and high particle density embedded on a hierarchical Al_2O_3 matrix, which exhibited improved activity and stability simultaneously toward the reaction of CO_2 methanation. The structural characterizations and catalytic evaluations demonstrated the existence of abundant surface-defected vacancy clusters of Ni nanoparticles (**Figure 10**), accounting for the significantly-enhanced low temperature activity of CO_2 methanation reaction. In addition, the anchoring effect from the support gives rise to a high reaction stability, without obvious aggregation of active species during long-term use. By virtue of the wide versatility of LDH composition and architecture, various single metal nanocatalysts with high dispersion and good thermal stability have been reported via reduction of LDH precursors.[59]

The addition of a second metal element to build bimetallic alloy catalysts with tunable geometric/electronic structure of metal active sites is an effective route to improve the catalytic behavior of supported metal catalysts. By incorporation of two VIII elements in LDH precursors, supported alloy catalysts can also be obtained by the topological transformation process. Wang et al.[60] reported the synthesis of CoFe/MgO nanocomposites from CoMgFe–LDH precursors via a H_2 gas-phase reduction, in which the Co/Fe ratio can be freely controlled by changing the chemical composition of LDH precursors. Subsequently, the NiFe alloy materials as catalysts toward the steam reforming of toluene or $N_2H_4{\cdot}H_2O$ decomposition for hydrogen generation have also been developed from LDH precursors by Tomishige et al.[61] and Wei et al.,[62] respectively. The remarkable Ni–Fe synergistic effect (formation of Ni–Fe chemical bond and their electron interaction) was believed to impose great impact on their catalytic behavior. In addition, for the metal element that can not be largely incorporated into the LDH host layers such as the noble metal Rh, their alloy nanocomposites can be fabricated via a bottom-up method. Recently, our group[63] further fabricated supported Ni@(RhNi-alloy)/Al_2O_3 nanocomposites involving the following three steps: (1) preparation of supported Ni NPs on an Al_2O_3 substrate (Ni/Al_2O_3) from a hierarchical NiAl–LDH precursor; (2) chemical etching of Ni/Al_2O_3 by $RhCl_3$ solution to obtain Ni@Rh/Al_2O_3; (3) calcination of Ni@Rh/Al_2O_3 to achieve the final Ni@(RhNi-alloy)/Al_2O_3 nanocomposite. The Ni core–(RhNi-alloy) shell NPs supported on the Al_2O_3 matrix show satisfactory catalytic performances toward hydrogen generation from $N_2H_4BH_3$ (HB) (5.74 ± 0.2 equiv. (H_2 + N_2) per HB within 40 min), taking the advantages of the defect-rich surface and

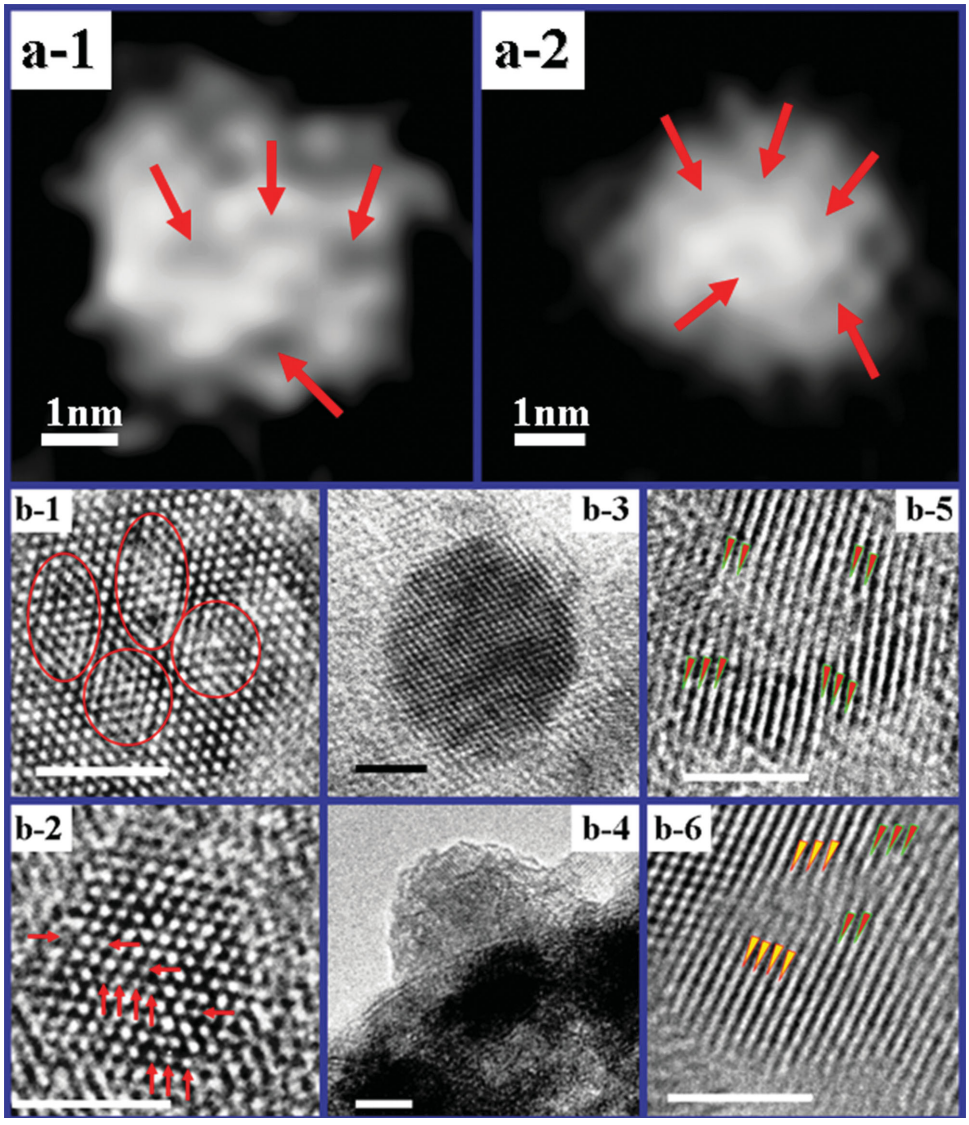

Figure 10. (a-1 and a-2) High-angle annular dark field (HAADF) STEM images of Ni nanoparticles in the sample of Ni/H–Al_2O_3(400). (b-1 to b-6) HRTEM images of Ni nanoparticles selected from the Ni/H–Al_2O_3(400) sample (the scale bar is 2 nm). Reproduced with permission.[58] Copyright 2013, American Chemical Society.

high utilization of noble metals in the unique core–shell alloy structure.

Compared with the alloy catalysts, the intermetallic compounds (IMCs) can be defined as a chemical compound of two or more metallic elements with a specific composition and definite crystal structure that differs from those of the constituent metals, which have attracted extensive research interest in catalysis owing to their unique electronic structures and the "active-site isolation" effect in recent years.[64] However, the synthesis process of IMCs is always high energy-intensive or not environmentally friendly. For the hydrotalcite approach, the advantage is that divalent and trivalent cations are uniformly distributed in slabs of edge-sharing MO_6 octahedra that allow a close interaction of different metal cations, which is the prerequisite to the uniform formation of IMCs.[65] Schlögl and Armbrüster[64b] even remark that the hydrotalcite approach does not rely on air-sensitive and expensive reactants, which serves as an industrially feasible synthesis for supported materials. Indeed, many new types of IMCs with improved catalytic performance have been developed through hydrotalcite approach, e.g., PdGa IMCs for alkane dehydrogenation,[66] PdIn IMCs for ethane and propane dehydrogenation,[67] PdGa and PdZn IMCs for methanol steam reforming and methanol synthesis from CO_2.[65] Most recently, Li et al.[68] reported the synthesis of the supported Pd-Ga IMC catalysts by reducing the $PdCl_4^{2-}$ intercalated MgGaAl-LDHs/Al_2O_3 (**Figure 11**), resulting in the intermetallic Pd–Ga/MgO–Al_2O_3. The catalysts exhibit comparable activity but much preferable selectivity in comparison with monometallic Pd/MgO–Al_2O_3 catalyst in the partial hydrogenation of acetylene, which can be attributed to the geometric effect and electronic effect between Pd and Ga, as revealed by XPS and CO-IR analysis.

By virtue of the tunable element ratio in hydroxide layers, the geometric and electronic structure of active sites can

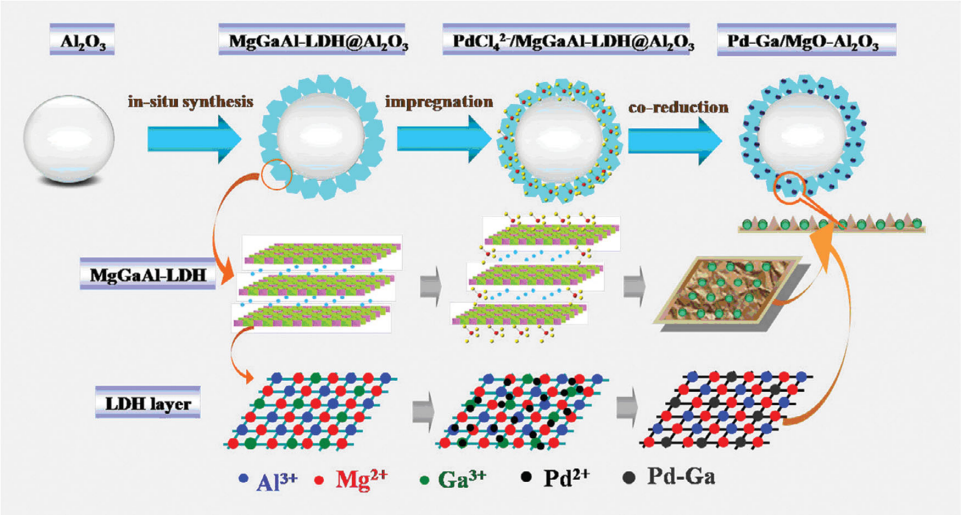

Figure 11. Synthetic schematic diagram of the novel supported bimetallic Pd–Ga catalysts from the LDH precursor approach. Reproduced with permission.[68] Copyright 2014, Elsevier.

be precisely controlled. Our group[69] recently reported the preparation of several supported Ni–In IMCs (Ni_3In, Ni_2In, NiIn and Ni_2In_3) with a tunable particle size based on the topological transformation of LDH precursors, which exhibit largely-enhanced catalytic activity and selectivity toward the hydrogenation of α,β-unsaturated aldehydes. The LDH precursor plays a key role in the synthesis of supported Ni-In IMCs: the atom-scale interspersion of components in LDHs facilitates the formation of highly-dispersed Ni-In IMCs with tunable Ni/In ratio and particle size. The decreased Ni–Ni coordination was observed with the increase of In/Ni ratio (**Figure 12**), resulting in an adjustable electronic and geometry structure of metal active sites. The catalytic evaluations show these supported Ni-In IMCs exhibit excellent catalytic activity and selectivity towards hydrogenation of unsaturated carbonyl compounds (e.g., furfural, 1-phenyltanol, crotonaldehyde, 2-hexenal) by the modulation of chemical composition and particle size of Ni-In IMCs. The XAFS characterization and DFT calculation further reveal the electron transfer from In to Ni atom and active-site isolation, which favors the nucleophilic addition process of C=O group other than the electrophilic addition of C=C, accounting for the largely-enhanced hydrogenation selectivity over Ni-In IMCs. Since most of the transition metals (e.g., Fe, Co, Ni, Cu, Zn), many main group elements (e.g., Mg, Al, Ga, In) and some noble metals can be incorporated into the lamellar LDH flake, the topological transformation procedure is promising for the fabrication of various supported monometallic, bimetal alloy or IMCs with high density, good stability and unique surface structure as efficient catalysts.

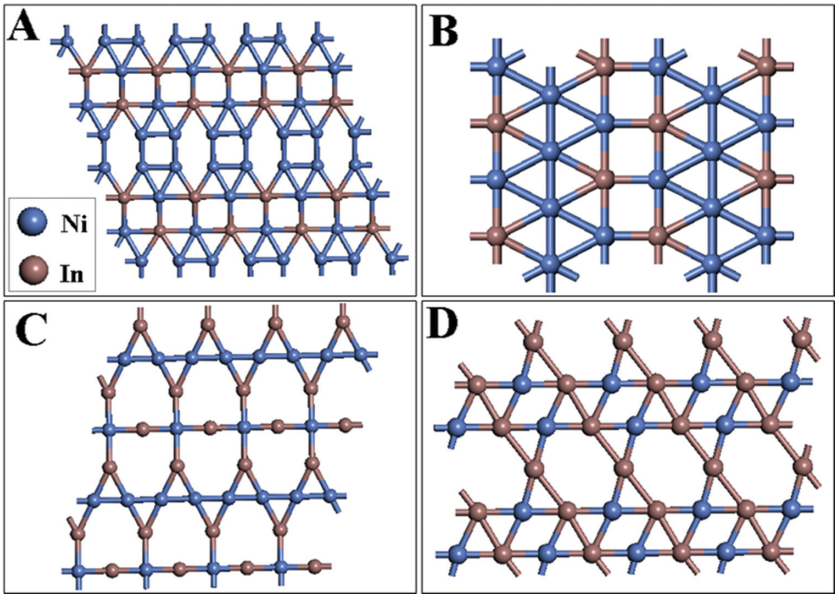

Figure 12. The atomic arrangement and chemical bonding of the preferential crystal face of Ni-In IMCs: (A) Ni_3In (201) face, (B) Ni_2In (110) face, (C) NiIn (201) face, (D) Ni_2In_3 (110) face. Reproduced with permission.[69] Copyright 2013, American Chemical Society.

4. LDH-Based Nanomaterials as Adsorbents

Widespread contamination of fresh water and atmosphere systems has become one of the forefront environmental problems.[70] The development of high-efficiency and recyclable absorbent nanomaterial is the great urgency to deal with various environmental pollutants (e.g., dye wastewater, heavy metal ion) and the greenhouse gases such as CO_2. For LDH materials as adsorbents, various structural units on LDHs (e.g., positive ion or basic sites) provide specific active sites for many adsorbates with strong chemical affinity. The facile manipulation of adsorption sites (e.g., electronic density, alkaline intensity) at the atomic scale as well as the

NANO MICRO small

morphology/pore structure at micron-nano scale gives the possibility to tune the active structure and adsorption kinetics for a specific adsorption process. Generally, the MMO materials derived from LDHs show largely-enhanced adsorption capacity owing to the increased specific surface area.[71] These features make LDH-based nanomaterials have a wide use as adsorbents.

4.1. LDH-Based Adsorbents in Adsorption and Separation

Recently, LDH materials have been developed as adsorbents for various organic dye molecules, including the adsorption of acid orange 10 over MgAl-LDHs,[72] sunset yellow FCF food dye over CaAl-LDH-NO_3,[73] methylene blue (MB), methyl orange (MO) and formaldehyde over ZnCr- and MgAl-LDHs.[74] The metal element in host layers, M^{2+}/M^{3+} ratio, interlayer anion and specific surface area were found to have influences on their adsorption behavior. Moreover, the fabrication of LDHs with high specific surface is another effective method to increase the adsorption capacity for dyes. We[75] developed several hierarchical LDH films with increased specific surface via an in situ growth or electrophoretic deposition process as structured adsorbent for water treatment. LDH films with 3D architectures composed of submicron features can be obtained over many man-made supports (paper, cloth, sponge, aluminum foam). The obtained films show improved adsorption capacity and ability to remove sulforhodamine B, Congo red, Remazol Brilliant Blue R in water treatment. An additional merit of the monolithic adsorbents is their facile sorption-regeneration property compared with the powdered samples, which facilitates repeatable and cyclic usage over a long period. In addition, the porous structure of the hierarchical LDHs is preferable for a better adsorption performance. Tokudome et al.[76] reported the control of macrochannel and mesochannel characteristics of LDH–$Al(OH)_3$ monolithic xerogels by tuning the phase separated structure and improving crystal growth. The resulting LDH–$Al(OH)_3$ monolithic xerogels with hierarchical channels exhibit controllable adsorption properties for pyranine and Rhodamine B. Qian and Xu's group[77] further studied the adsorption kinetics of arsenate and phosphate over LDH materials. It was found that removal of these anions from aqueous solution follows the Lagergren first-order and/or pseudo-second-order model, and the adsorption isotherm is well fitted with either the Langmuir or the Freundlich model. Most recently, O'Hare and Wang[78] developed the aqueous miscible organic solvent treatment (AMOST) method to synthesize highly-porous and highly-dispersed LDHs with large specific surface. The Zn_2Al-borate and Mg_3Al-borate LDH powdered samples containing exfoliated nanosheets have extremely high specific surface area (458.6 and 263 $m^2\ g^{-1}$, respectively). The ultrahigh surface area LDHs prepared using this approach will have immediate and substantial impact for LDHs as sorbents.

The fabrication of hierarchical/porous LDH nanomaterials with a high specific surface area is also effective for adsorption of heavy metal or inorganic ions in waste water (e.g., Cr^{VI}, arsenate, boron, fluoride, or phosphate).[75c,79] Furthermore, the combination of LDHs with other functional materials can further improve the adsorption efficiency together with some new functionality. Zhang et al.[80] reported the anisotropic LDH nanocrystals@carbon nanosphere via direct assembly of anisotropic LDHs onto the surface of carbon nanospheres. It was found that the maximum adsorption capacity of the nanocomposite toward Cu^{2+} was ~19.93 mg g^{-1} when the initial Cu^{2+} concentration was 10.0 mg L^{-1}, displaying a high efficiency for the removal of heavy metal ions. Xu and Wang et al.[79a] recently developed the LDH/graphene oxide (GO) nanocomposites via a hydrothermal synthesis process, which exhibited swelling behavior in water to form a gel. The GO/LDHs ratio significantly affected the adsorption capacity for As(V), with a maximum adsorption capacity of 183.11 mg/g over the nanocomposites containing 6.0% GO due to the higher Brunauer–Emmett–Teller (BET) surface area. Moreover, the incorporation of magnetism motif with LDHs provides additional magnetic separation function for LDH adsorbents, e.g., MgAl-LDH nanoflake impregnated magnetic alginate beads (LDH-n-MABs) for the removal of fluoride in water[81] and Fe_3O_4@C@LDH for magnetic separation of uranium.[82] Our group[83] reported the combination of magnetic Fe_3O_4 with hierarchical LDHs to form the Fe_3O_4@SiO_2@LDH microspheres for magnetic separation of proteins (**Figure 13**). The Ni^{2+} cations in the NiAl-LDH shell provide docking sites for histidine and the materials exhibit good performance in the separation of a histidine (His)-tagged green fluorescent protein, with a binding capacity as high as 239 μg/mg. The microspheres show highly-selective adsorption of the His-tagged protein from Escherichia coli lysate, demonstrating their practical applicability. Moreover, the microspheres possess superparamagnetism and high saturation magnetization (36.8 emu/g), which allows them to be easily separated from solution by means of an external magnetic field for subsequent reuse. In addition, the formation of mixed metal oxides (MMOs) from the topological transformation of LDH precursors generally increases the specific surface area markedly. Correspondingly, the adsorption capacity for both organic dyes and inorganic ions can be further improved such as in the cases of adsorption of acid brown 14 dye on MgFe-MMO with memory effect,[84] acid green or thiosulfate over MgAl-MMO,[85] methyl orange over rGO/Ni/MMO hybrid.[71] This structure feature significantly enhances the functionality and performance of LDH-based materials as adsorbents.

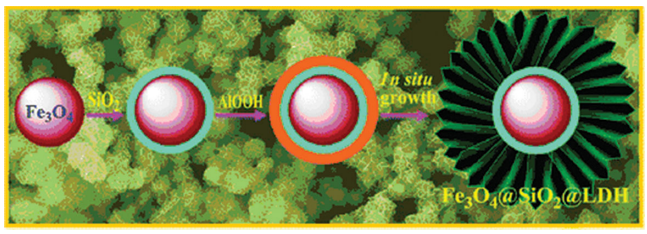

Figure 13. The synthetic schematic diagram of Fe_3O_4@SiO_2@LDHs core–shell microspheres for magnetic separation of proteins. Reproduced with permission.[83] Copyright 2011, American Chemical Society.

The desorption of adsorbates from adsorbent materials is the key problem for their cyclic utilization. To remove the adsorbates, several methods have been explored, e.g., washing used LDH adsorbents with alkaline solutions (such as NaOH), salt solutions (NaCl, $FeCl_2$, Na_2CO_3, and $NaHCO_3$) or a mixture of these solutions via the anion exchange process, acid treatment method, calcination and reconstruction process between LDHs and MMOs.[86] However, these treatments often suffer from changing the initial structure and surface state of LDHs with the introduction of impurities, resulting in unsatisfactory recyclable performances. Given the strong affinity of CO_2 to LDHs, Lin et al.[87] recently investigated desorption and enrichment of Cr^{VI} from Cr^{VI}-LDH as well as recycling of LDH in the presence of high-pressure CO_2. It was found that Cr^{VI} solution with a concentration of 500 mg/L could be enriched more than 20 times in each adsorption–desorption cycle. Notably, a pilot-scale experiment was carried out with 20 L Cr^{VI}-containing electroplating wastewater, and the concentration of desorbed Cr^{VI} solution enriched to 10 000 mg/L, which could be used in electroplating after appropriate treatment. This method shows the advantages of desorption behavior at high Cr^{VI} concentration, direct reuse of enriched Cr^{VI}, and efficient regeneration of LDH adsorbent, which can serve as a promising approach in the treatment of industrial wastewater.

4.2. MMOs as Adsorbents for CO_2 Capture

Recently, CO_2 emission has become a serious problem such as global warming and climate change due to the combustion of fossil fuels. The capture and separation of CO_2 over adsorbents prior to emission into the environment is one of the main technological strategies to control CO_2 concentration.[88] An excellent sorbent should have high sorption capacity, long-term durability, rapid adsorption/desorption rate, and good mechanical strength under high temperature conditions such as in the integrated gasification combined cycle (IGCC).[89]

For MMO materials derived from the calcination of LDHs, the alkaline component (e.g., MgO, CaO) in MMOs serves as the active species for the adsorption of acidic CO_2 molecule. Among various CO_2 adsorbents, the MMO materials have been identified as the most suitable one for CO_2 capture in the high temperature range. To date, many studies have been performed on LDH-derived CO_2 adsorbents with great progress by virtue of intrinsic features of LDH precursors, for instance, the type and ratio of divalent and trivalent cations,[90] charge compensating anions,[91] morphology/particle size,[92] alkali metal (K, Cs) doping[93] as well as the adsorption/desorption kinetics.[93,94] For further improved adsorption performance, the assembly of LDHs with other advanced materials to form nanocomposites may open a new way to fabricate LDH-based absorbent materials with high efficiency such as in the cases of LDHs/graphene oxide[95] and LDHs/mesoporous AlOOH[96] system. Most recently, Giannelis and Eddaoudi et al.[97] reported the synthesis of hierarchical mesostructure MgAl-LDHs via confined growth on mesoporous silica foams by simple impregnation and hydrothermal treatment. The as-synthesized LDH/silica foam nanocomposites show well-defined mesostructure with a high surface area, large pore volume, and mesopores of 6–7 nm, which exhibit significantly-enhanced CO_2 capacity with high CO_2/N_2 and CO_2/CH_4 selectivity under high-pressure conditions.

A deep insight into the structure of the active sites and mechanism for CO_2 adsorption would shed light on the synthesis and utilization of LDH-derived high temperature CO_2 adsorption materials with enhanced performance. In general, the basic sites in these materials are regarded as the adsorption center for the acid CO_2 molecule. Reddy et al.[98] reported that a calcination temperature of 400 °C for LDH materials is necessary for the highest CO_2 adsorption capacity, and proposed that Mg–O serves as the basic site. By comparison of different Mg–M–CO_3 (M = Al, Fe, Ga, Mn) LDH processors for high-temperature CO_2 capture, Wang et al.[99] also demonstrated that the M^{3+} ion determines the structure evolution of LDH derivatives under thermal treatment, and finally influences the CO_2 capture capacity. Recently, they[100] further systematically investigated the effects of precipitation agent, preparation method, Mg/Al ratio, pretreatment conditions, adsorption conditions on the CO_2 adsorption capacity, and gave the possible CO_2 adsorption sites and mechanism for LDH-derived metal oxides by carefully examining the structural changes during the thermal treatment via XRD and solid state NMR. It was proposed that the active Mg–O species might be induced either by the substitution of Mg^{2+} by Al^{3+} in periclase (MgO lattice), or by the diffusion of Al^{3+} out of the octahedral brucite layers (**Figure 14**).

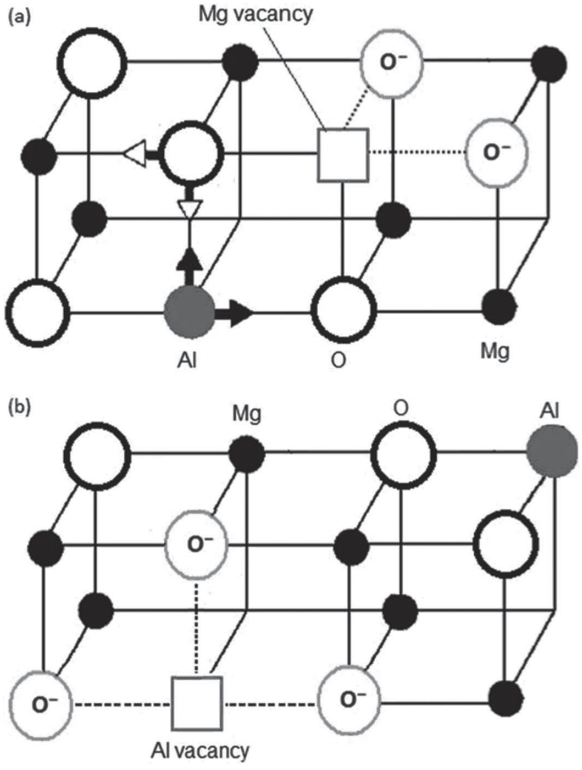

Figure 14. The proposed mechanisms for the formation of active Mg–O species induced by (a) the substitution of Mg by Al and (b) the diffusion of Al atoms out of the octahedral brucite layers. Reproduced with permission.[100] Copyright 2013, Royal Society of Chemistry.

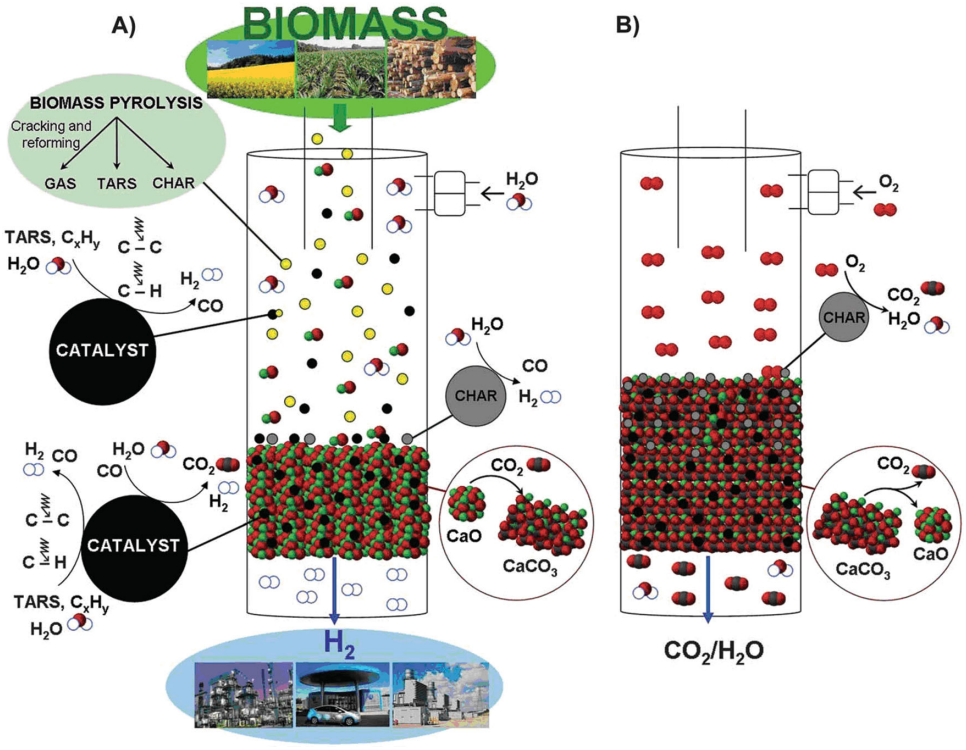

Figure 15. Scheme of the reaction routes during consecutive stages of sorption enhanced catalytic steam gasification (SECSG) (A) and sorbent regeneration (B). Reproduced with permission.[101] Copyright 2012, Royal Society of Chemistry.

In some cases, the CO_2 adsorption can be coupled with the subsequent reaction with largely-improved catalytic performances together with the CO_2 capture function. A typical example is the sorption-enhanced water gas shift (SEWGS) process, which is a combination of CO_2 adsorption and the WGS reaction. By adsorbing and removing CO_2 from the reaction mixture over adsorption materials such as MMOs, the reaction is driven to the right-hand-side, thereby completely converting CO and maximizing the production of H_2.[92] By the utilization of both the adsorption and the catalytic function of LDH-based materials, Chen et al.[101] reported the synthesis of Pd/Co–Ni catalyst derived from the LDHs and dolomite toward one-stage hydrogen production from raw solid lignocellulosic biomass by sorption-enhanced catalytic steam gasification (SECSG) (**Figure 15**). Almost pure hydrogen (>99.9 vol%) and high H_2 yields (up to 90%) can be achieved by this process, which combines conventional gasification/steam reforming, water-gas shift (WGS) reaction and H_2 separation by CO_2 capture in one step. The in situ removal of CO_2 by the carbonation reaction of dolomite shifts the equilibrium of steam reforming and WGS reactions towards H_2 production. Recently, Müller et al.[102] also developed the LDH-based Ni-Ca bifunctional sorbent/catalyst for the sorbent-enhanced steam methane reforming (SE-SMR) reaction. The Ni reforming catalyst and the Ca-based CO_2 sorbent can be obtained by the reduction of $(Al:Ca:Mg:Ni)O_x$ mixed metal oxides into nickel and CaO particles supported on the Al_2O_3-MgO matrix with a surface area of 54 $m^2 \cdot g^{-1}$. The nanocomposites produce a larger amount of high-purity H_2 than limestone mixed with Ni/SiO_2 or $nickel/Al_2O_3$-MgO catalysts owing to the synergy between the adsorption and the catalysis process. Nevertheless, many challenges are still involved in this process, such as the catalyst activity/stability, the compatibility of the catalyst with CO_2 acceptors, and the reactor design. Appropriate resolutions to these problems would provide a unique opportunity for the development of innovative processing technology for the production of new clean energy.

5. Conclusion

In this review, we summarized the recent progress in the design and preparation of LDH-based materials as catalysts and sorbents, in the fields of photocatalysis/photoelectrocatalysis, heterogeneous catalysis, adsorption and separation of pollutants or greenhouse gases. By virtue of the versatility of LDH materials (chemical composition, size and morphology) as well as their unique features (intercalation/delamination, topological transformation and self-assembly with other functional materials), a series of LDH-based nanomaterials have been designed and fabricated to satisfy specific catalytic and adsorbent processes. Important research contributions are highlighted to illustrate the manipulation of both the active sites (e.g., crystal face, defect, geometry and electronic state, etc.) and macro-nano morphology with enhanced performance for their potential industrial applications. Although much progress has been made, great challenges still remain in the preparation and application of LDH-based nanomaterials as catalysts/sorbents: (i) it is always a conundrum to

identify the active center structure, especially in the LDH-based nanocomposites, which would restrict the purposed design and control synthesis of nanomaterials with desired active sites; (ii) although satisfactory performances over LDH-based materials have been achieved, the catalytic/adsorptive mechanism is another challenge deserving deeper study for further improvement of functionality; (iii) the lattice orientation/lattice confinement effect during the reversible topotactic transformation/reconstruction process of LDH materials has not been well understood to date and more detailed and thorough investigations are needed. In the further study, the innovation of synthetic strategies and assembly of LDHs with other functional materials would open new room for LDH-based nanometerials in catalysis/adsorption. In addition, the application of in situ characterization technique and tracer technique would also be great help to understand both the active center structure and catalytic/adsorptive mechanism for the purpose of achieving more rational material design. With the rapid advance in synthetic and characteristic strategies of nanoscience and nanotechnology, the design and controlled synthesis of LDH-based functional nanomaterials would make a great contribution to sustainable development in the field of catalysis/adsorption.

Acknowledgements

This work was supported by the 973 Program (Grant no.: 2011CBA00504), the National Natural Science Foundation of China (NSFC), the Scientific Fund from Beijing Municipal Commission of Education (20111001002) and the Fundamental Research Funds for the Central Universities (ZD 1303). M. Wei particularly appreciates the financial aid from the China National Funds for Distinguished Young Scientists of the NSFC.

[1] a) J. Liu, S. Z. Qiao, Q. H. Hu, G. Q. Lu, *Small* **2011**, *7*, 425; b) G. A. Somorjai, H. Frei, J. Y. Park, *J. Am. Chem. Soc.* **2009**, *131*, 16589; c) G. J. Hutchings, M. Brust, H. Schmidbaur, *Chem. Soc. Rev.* **2008**, *37*, 1759; d) R. Schlögl, S. B. Abd Hamid, *Angew. Chem. Int. Ed.* **2004**, *43*, 1628; e) A. R. Tao, S. Habas, P. Yang, *Small* **2008**, *4*, 310.

[2] a) A. T. Bell, *Science* **2003**, *299*, 1688; b) K. Zhou, Y. Li, *Angew. Chem. Int. Ed.* **2012**, *51*, 602; c) P. Yang, S.-Y. Jin, Q.-Z. Xu, S.-H. Yu, *Small* **2013**, *9*, 199; d) X. Huang, C. Guo, J. Zuo, N. Zheng, G. D. Stucky, *Small* **2009**, *5*, 361.

[3] a) J.-M. Song, S.-S. Zhang, S.-H. Yu, *Small* **2014**, *10*, 717; b) L. J. Giovanetti, J. M. Ramallo-López, M. Foxe, L. C. Jones, M. M. Koebel, G. A. Somorjai, A. F. Craievich, M. B. Salmeron, F. G. Requejo, *Small* **2012**, *8*, 468.

[4] a) A. M. Fogg, A. L. Rohl, G. M. Parkinson, D. O'Hare, *Chem. Mater.* **1999**, *11*, 1194; b) J. A. Gursky, S. D. Blough, C. Luna, C. Gomez, A. N. Luevano, E. A. Gardner, *J. Am. Chem. Soc.* **2006**, *128*, 8376; c) G. R. Williams, D. O'Hare, *J. Mater. Chem.* **2006**, *16*, 3065; d) V. Rives, M. a. Angeles Ulibarri, *Coord. Chem. Rev.* **1999**, *181*, 61; e) Z. P. Xu, J. Zhang, M. O. Adebajo, H. Zhang, C. Zhou, *Appl. Clay Sci.* **2011**, *53*, 139.

[5] Q. Wang, D. O'Hare, *Chem. Rev.* **2012**, *112*, 4124.

[6] C. Li, J. Zhou, W. Gao, J. Zhao, J. Liu, Y. Zhao, M. Wei, D. G. Evans, X. Duan, *J. Mater. Chem. A* **2013**, *1*, 5370.

[7] Y. Zhao, M. Wei, J. Lu, Z. L. Wang, X. Duan, *ACS Nano* **2009**, *3*, 4009.

[8] L. Tian, Y. Zhao, S. He, M. Wei, X. Duan, *Chem. Eng. J.* **2012**, *184*, 261.

[9] M.-Q. Zhao, Q. Zhang, W. Zhang, J.-Q. Huang, Y. Zhang, D. S. Su, F. Wei, *J. Am. Chem. Soc.* **2010**, *132*, 14739.

[10] a) X. Chen, S. Shen, L. Guo, S. S. Mao, *Chem. Rev.* **2010**, *110*, 6503; b) I. Paramasivam, H. Jha, N. Liu, P. Schmuki, *Small* **2012**, *8*, 3073; c) J. Liu, G. Zhang, *Phys. Chem. Chem. Phys.* **2014**, *16*, 8178.

[11] C. G. Silva, Y. Bouizi, V. Fornés, H. García, *J. Am. Chem. Soc.* **2009**, *131*, 13833.

[12] S. J. Kim, Y. Lee, D. K. Lee, J. W. Lee, J. K. Kang, *J. Mater. Chem. A* **2014**, *2*, 4136.

[13] N. Baliarsingh, L. Mohapatra, K. Parida, *J. Mater. Chem. A* **2013**, *1*, 4236.

[14] K. Parida, M. Satpathy, L. Mohapatra, *J. Mater. Chem.* **2012**, *22*, 7350.

[15] a) Y. Zhao, P. Chen, B. Zhang, D. S. Su, S. Zhang, L. Tian, J. Lu, Z. Li, X. Cao, B. Wang, M. Wei, D. G. Evans, X. Duan, *Chem.—Eur. J.* **2012**, *18*, 11949; b) Y. Zhao, S. Zhang, B. Li, H. Yan, S. He, L. Tian, W. Shi, J. Ma, M. Wei, D. G. Evans, X. Duan, *Chem.—Eur. J.* **2011**, *17*, 13175.

[16] Y. Zhao, B. Li, Q. Wang, W. Gao, C. J. Wang, M. Wei, D. G. Evans, X. Duan, D. O'Hare, *Chem. Sci.* **2014**, *5*, 951.

[17] a) N. Ahmed, Y. Shibata, T. Taniguchi, Y. Izumi, *J. Catal.* **2011**, *279*, 123; b) M. Morikawa, N. Ahmed, Y. Yoshida, Y. Izumi, *Appl. Catal. B* **2014**, *144*, 561.

[18] K. Teramura, S. Iguchi, Y. Mizuno, T. Shishido, T. Tanaka, *Angew. Chem. Int. Ed.* **2012**, *51*, 8008.

[19] J. S. Valente, F. Tzompantzi, J. Prince, *Appl. Catal. B* **2011**, *102*, 276.

[20] J. L. Gunjakar, T. W. Kim, H. N. Kim, I. Y. Kim, S.-J. Hwang, *J. Am. Chem. Soc.* **2011**, *133*, 14998.

[21] B. Li, Y. Zhao, S. Zhang, W. Gao, M. Wei, *ACS Appl. Mater. Interfaces* **2013**, *5*, 10233.

[22] J. L. Gunjakar, I. Y. Kim, J. M. Lee, N.-S. Lee, S.-J. Hwang, *Energy Environ. Sci.* **2013**, *6*, 1008.

[23] Z. Huang, P. Wu, B. Gong, Y. Fang, N. Zhu, *J. Mater. Chem. A* **2014**, *2*, 5534.

[24] S. He, S. Zhang, J. Lu, Y. Zhao, J. Ma, M. Wei, D. G. Evans, X. Duan, *Chem. Commun.* **2011**, *47*, 10797.

[25] a) J. Hong, Y. Wang, J. Pan, Z. Zhong, R. Xu, *Nanoscale* **2011**, *3*, 4655; b) K.-i. Katsumata, K. Sakai, K. Ikeda, G. Carja, N. Matsushita, K. Okada, *Mater. Lett.* **2013**, *107*, 138; c) G. Carja, M. Birsanu, K. Okada, H. Garcia, *J. Mater. Chem. A* **2013**, *1*, 9092.

[26] F. E. Osterloh, *Chem. Soc. Rev.* **2013**, *42*, 2294.

[27] M. Shao, F. Ning, M. Wei, D. G. Evans, X. Duan, *Adv. Funct. Mater.* **2014**, *24*, 580.

[28] S. Cho, J.-W. Jang, K.-j. Kong, E. S. Kim, K.-H. Lee, J. S. Lee, *Adv. Funct. Mater.* **2013**, *23*, 2348.

[29] T. J. Pinnavaia, *Science* **1983**, *220*, 365.

[30] V. Polshettiwar, R. S. Varma, *Green Chem.* **2010**, *12*, 743.

[31] B. Sels, D. D. Vos, M. Buntinx, F. Pierard, A. Kirsch-De Mesmaeker, P. Jacobs, *Nature* **1999**, *400*, 855.

[32] B. M. Choudary, B. Bharathi, C. V. Reddy, M. L. Kantam, K. V. Raghavan, *Chem. Commun.* **2001**, *37*, 1736.

[33] S. Zhao, J. Xu, M. Wei, Y.-F. Song, *Green Chem.* **2011**, *13*, 384.

[34] B. F. Sels, D. E. De Vos, P. A. Jacobs, *J. Am. Chem. Soc.* **2007**, *129*, 6916.

[35] a) P. Liu, H. Wang, Z. Feng, P. Ying, C. Li, *J. Catal.* **2008**, *256*, 345; b) P. Liu, C. Wang, C. Li, *J. Catal.* **2009**, *262*, 159.

[36] M. Wei, X. Zhang, D. G. Evans, X. Duan, *AIChE J.* **2007**, *53*, 2916.

[37] S. Bhattacharjee, T. J. Dines, J. A. Anderson, *J. Phy. Chem. C* **2008**, *112*, 14124.

[38] K. M. Parida, M. Sahoo, S. Singha, *J. Catal.* **2010**, *276*, 161.
[39] K. A. D. d. F. Castro, A. Bail, P. B. Groszewicz, G. S. Machado, W. H. Schreiner, F. Wypych, S. Nakagaki, *Appl. Catal. A* **2010**, *386*, 51.
[40] T. C. O. Mac Leod, M. N. Kopylovich, M. F. C. Guedes da Silva, K. T. Mahmudov, A. J. L. Pombeiro, *Appl. Catal. A* **2012**, *439–440*, 15.
[41] I. Cota, E. Ramírez, F. Medina, J. E. Sueiras, G. Layrac, D. Tichit, *Appl. Catal. A* **2010**, *382*, 272.
[42] S. Bhattacharjee, J. A. Anderson, *Chem. Commun.* **2004**, *40*, 554.
[43] a) H. Liu, L. Zhao, J. Wang, J. He, *J. Catal.* **2013**, *298*, 70; b) H. Shi, J. He, *J. Catal.* **2011**, *279*, 155; c) J. Wang, L. Zhao, H. Shi, J. He, *Angew. Chem. Int. Ed.* **2011**, *50*, 9171.
[44] X.-F. Yang, A. Wang, B. Qiao, J. Li, J. Liu, T. Zhang, *Acc. Chem. Res.* **2013**, *46*, 1740.
[45] Z. Yang, W. W. Tjiu, W. Fan, T. Liu, *Electrochim. Acta* **2013**, *90*, 400.
[46] X.-Y. Ma, Y.-Y. Chai, D. G. Evans, D.-Q. Li, J.-T. Feng, *J. Phy. Chem. C* **2011**, *115*, 8693.
[47] F. Zhang, X. Zhao, C. Feng, B. Li, T. Chen, W. Lu, X. Lei, S. Xu, *ACS Catal.* **2011**, *1*, 232.
[48] J. H. Lee, H. Kim, Y. S. Lee, D.-Y. Jung, *ChemCatChem* **2014**, *6*, 113.
[49] a) F. Basile, G. Fornasari, M. Gazzano, A. Vaccari, *J. Mater. Chem.* **2002**, *12*, 3296; b) K. Kaneda, T. Yamashita, T. Matsushita, K. Ebitani, *J. Org. Chem.* **1998**, *63*, 1750; c) K. Kaneda, K. Yamaguchi, K. Mori, T. Mizugaki, K. Ebitani, *Catal. Surv. Jpn.* **2000**, *4*, 31; d) T. Matsushita, K. Ebitani, K. Kaneda, *Chem. Commun.* **1999**, *35*, 265.
[50] X. Zou, A. Goswami, T. Asefa, *J. Am. Chem. Soc.* **2013**, *135*, 17242.
[51] P. Liu, Y. Guan, R. A. v. Santen, C. Li, E. J. M. Hensen, *Chem. Commun.* **2011**, *47*, 11540.
[52] L. Li, L. Dou, H. Zhang, *Nanoscale* **2014**, *6*, 3753.
[53] S. He, Z. An, M. Wei, D. G. Evans, X. Duan, *Chem. Commun.* **2013**, *49*, 5912.
[54] G.-L. Tian, M.-Q. Zhao, B. Zhang, Q. Zhang, W. Zhang, J.-Q. Huang, T.-C. Chen, W.-Z. Qian, D. S. Su, F. Wei, *J. Mater. Chem. A* **2014**, *2*, 1686.
[55] L. He, Y. Huang, A. Wang, X. Wang, X. Chen, J. J. Delgado, T. Zhang, *Angew. Chem. Int. Ed.* **2012**, *51*, 6191.
[56] S. Velu, K. Suzuki, M. P. Kapoor, S. Tomura, F. Ohashi, T. Osaki, *Chem. Mater.* **2000**, *12*, 719.
[57] C. Li, Y. Chen, S. Zhang, J. Zhou, F. Wang, S. He, M. Wei, D. G. Evans, X. Duan, *ChemCatChem* **2014**, *6*, 824.
[58] S. He, C. Li, H. Chen, D. Su, B. Zhang, X. Cao, B. Wang, M. Wei, D. G. Evans, X. Duan, *Chem. Mater.* **2013**, *25*, 1040.
[59] a) X. Xiang, H. I. Hima, H. Wang, F. Li, *Chem. Mater.* **2007**, *20*, 1173; b) J. Feng, X. Ma, Y. He, D. G. Evans, D. Li, *Appl. Catal. A* **2012**, *413–414*, 10.
[60] L. Wang, J. Liu, Y. Zhou, Y. Song, J. He, D. G. Evans, *Chem. Commun.* **2010**, *46*, 3911.
[61] M. Koike, D. Li, Y. Nakagawa, K. Tomishige, *ChemSusChem* **2012**, *5*, 2312.
[62] W. Gao, C. Li, H. Chen, M. Wu, S. He, M. Wei, D. G. Evans, X. Duan, *Green Chem.* **2014**, *16*, 1560.
[63] C. Li, Y. Dou, J. Liu, Y. Chen, S. He, M. Wei, D. G. Evans, X. Duan, *Chem. Commun.* **2013**, *49*, 9992.
[64] a) C. Xiao, L.-L. Wang, R. V. Maligal-Ganesh, V. Smetana, H. Walen, P. A. Thiel, G. J. Miller, D. D. Johnson, W. Huang, *J. Am. Chem. Soc.* **2013**, *135*, 9592; b) M. Armbrüster, K. Kovnir, M. Behrens, D. Teschner, Y. Grin, R. Schlögl, *J. Am. Chem. Soc.* **2010**, *132*, 14745.
[65] A. Ota, E. L. Kunkes, I. Kasatkin, E. Groppo, D. Ferri, B. Poceiro, R. M. Navarro Yerga, M. Behrens, *J. Catal.* **2012**, *293*, 27.
[66] G. Siddiqi, P. Sun, V. Galvita, A. T. Bell, *J. Catal.* **2010**, *274*, 200.
[67] P. Sun, G. Siddiqi, W. C. Vining, M. Chi, A. T. Bell, *J. Catal.* **2011**, *282*, 165.
[68] Y. He, L. Liang, Y. Liu, J. Feng, C. Ma, D. Li, *J. Catal.* **2014**, *309*, 166.
[69] C. Li, Y. Chen, S. Zhang, S. Xu, J. Zhou, F. Wang, M. Wei, D. G. Evans, X. Duan, *Chem. Mater.* **2013**, *25*, 3888.
[70] L. Yang, Z. Shahrivari, P. K. T. Liu, M. Sahimi, T. T. Tsotsis, *Ind. Eng. Chem. Res.* **2005**, *44*, 6804.
[71] Z. Yang, S. Ji, W. Gao, C. Zhang, L. Ren, W. W. Tjiu, Z. Zhang, J. Pan, T. Liu, *J. Colloid Interf. Sci.* **2013**, *408*, 25.
[72] R. Extremera, I. Pavlovic, M. R. Pérez, C. Barriga, *Chem. Eng. J.* **2012**, *213*, 392.
[73] F. P. de Sá, B. N. Cunha, L. M. Nunes, *Chem. Eng. J.* **2013**, *215–216*, 122.
[74] X. Liu, X. Zhao, Y. Zhu, F. Zhang, *Appl. Catal. B* **2013**, *140–141*, 241.
[75] a) Y. Zhao, S. He, M. Wei, D. G. Evans, X. Duan, *Chem. Commun.* **2010**, *46*, 3031; b) S. He, Y. Zhao, M. Wei, X. Duan, *Ind. Eng. Chem. Res.* **2011**, *50*, 2800; c) S. He, Y. Zhao, M. Wei, D. G. Evans, X. Duan, *Ind. Eng. Chem. Res.* **2011**, *51*, 285.
[76] N. Tarutani, Y. Tokudome, K. Nakanishi, M. Takahashi, *RSC Adv.* **2014**, *4*, 16075.
[77] Y. Xu, Y. Dai, J. Zhou, Z. P. Xu, G. Qian, G. Q. M. Lu, *J. Mater. Chem.* **2010**, *20*, 4684.
[78] Q. Wang, D. O'Hare, *Chem. Commun.* **2013**, *49*, 6301.
[79] a) T. Wen, X. Wu, X. Tan, X. Wang, A. Xu, *ACS Appl. Mater. Interfaces* **2013**, *5*, 3304; b) E. D. Isaacs-Paez, R. Leyva-Ramos, A. Jacobo-Azuara, J. M. Martinez-Rosales, J. V. Flores-Cano, *Chem. Eng. J.* **2014**, *245*, 248; c) D. Kang, X. Yu, S. Tong, M. Ge, J. Zuo, C. Cao, W. Song, *Chem. Eng. J.* **2013**, *228*, 731.
[80] J. Gong, T. Liu, X. Wang, X. Hu, L. Zhang, *Environ. Sci. Technol.* **2011**, *45*, 6181.
[81] C. Gao, X.-Y. Yu, T. Luo, Y. Jia, B. Sun, J.-H. Liu, X.-J. Huang, *J. Mater. Chem. A* **2014**, *2*, 2119.
[82] X. Zhang, J. Wang, R. Li, Q. Dai, R. Gao, Q. Liu, M. Zhang, *Ind. Eng. Chem. Res.* **2013**, *52*, 10152.
[83] M. Shao, F. Ning, J. Zhao, M. Wei, D. G. Evans, X. Duan, *J. Am. Chem. Soc.* **2011**, *134*, 1071.
[84] Y. Guo, Z. Zhu, Y. Qiu, J. Zhao, *Chem. Eng. J.* **2013**, *219*, 69.
[85] a) R. M. M. dos Santos, R. G. L. Gonçalves, V. R. L. Constantino, L. M. da Costa, L. H. M. da Silva, J. Tronto, F. G. Pinto, *Appl. Clay Sci.* **2013**, *80–81*, 189; b) C. Geng, T. Xu, Y. Li, Z. Chang, X. Sun, X. Lei, *Chem. Eng. J.* **2013**, *232*, 510.
[86] a) Y. Xu, J. Zhang, G. Qian, Z. Ren, Z. P. Xu, Y. Wu, Q. Liu, S. Qiao, *Ind. Eng. Chem. Res.* **2010**, *49*, 2752; b) L. M. Parker, N. B. Milestone, R. H. Newman, *Ind. Eng. Chem. Res.* **1995**, *34*, 1196; c) Y. Li, B. Gao, T. Wu, D. Sun, X. Li, B. Wang, F. Lu, *Water Res.* **2009**, *43*, 3067.
[87] X. Lv, Z. Chen, Y. Wang, F. Huang, Z. Lin, *ACS Appl. Mater. Interfaces* **2013**, *5*, 11271.
[88] S. Choi, J. H. Drese, C. W. Jones, *ChemSusChem* **2009**, *2*, 796.
[89] D. P. Harrison, *Ind. Eng. Chem. Res.* **2008**, *47*, 6486.
[90] C. T. Yavuz, B. D. Shinall, A. V. Iretskii, M. G. White, T. Golden, M. Atilhan, P. C. Ford, G. D. Stucky, *Chem. Mater.* **2009**, *21*, 3473.
[91] Q. Wang, H. H. Tay, Z. Zhong, J. Luo, A. Borgna, *Energy Environ. Sci.* **2012**, *5*, 7526.
[92] Q. Wang, Y. Gao, J. Luo, Z. Zhong, A. Borgna, Z. Guo, D. O'Hare, *RSC Adv.* **2013**, *3*, 3414.
[93] S. Walspurger, L. Boels, P. D. Cobden, G. D. Elzinga, W. G. Haije, R. W. van den Brink, *ChemSusChem* **2008**, *1*, 643.
[94] M. R. Othman, N. M. Rasid, W. J. N. Fernando, *Chem. Eng. Sci.* **2006**, *61*, 1555.
[95] A. Garcia-Gallastegui, D. Iruretagoyena, V. Gouvea, M. Mokhtar, A. M. Asiri, S. N. Basahel, S. A. Al-Thabaiti, A. O. Alyoubi, D. Chadwick, M. S. P. Shaffer, *Chem. Mater.* **2012**, *24*, 4531.

[96] Y.-P. Chang, Y.-C. Chen, P.-H. Chang, S.-Y. Chen, *ChemSusChem* **2012**, *5*, 1249.
[97] L. Fu, G. Qi, O. Shekhah, Y. Belmabkhout, L. Estevez, M. Eddaoudi, E. P. Giannelis, *ChemSusChem* **2014**, *7*, 1035.
[98] M. K. Ram Reddy, Z. P. Xu, G. Q. Lu, J. C. Diniz da Costa, *Ind. Eng. Chem. Res.* **2006**, *45*, 7504.
[99] Q. Wang, H. H. Tay, D. J. W. Ng, L. Chen, Y. Liu, J. Chang, Z. Zhong, J. Luo, A. Borgna, *ChemSusChem* **2010**, *3*, 965.
[100] Y. Gao, Z. Zhang, J. Wu, X. Yi, A. Zheng, A. Umar, D. O'Hare, Q. Wang, *J. Mater. Chem. A* **2013**, *1*, 12782.
[101] J. Fermoso, F. Rubiera, D. Chen, *Energy Environ. Sci.* **2012**, *5*, 6358.
[102] M. Broda, A. M. Kierzkowska, D. Baudouin, Q. Imtiaz, C. Copéret, C. R. Müller, *ACS Catal.* **2012**, *2*, 1635.

Received: May 25, 2014
Revised: July 7, 2014
Published online: August 18, 2014